AD-A157 895 RADIATION FOG MODELLING(U) UNIVERSITY OF MANCHESTER INST OF SCIENCE AND TECHNOLOGY (ENGLAND) DEPT OF PHYSICS J LATHAM ET AL. SEP 82 DAJA37-81-C-0746 1/1

UNCLASSIFIED F/G 4/2 NL

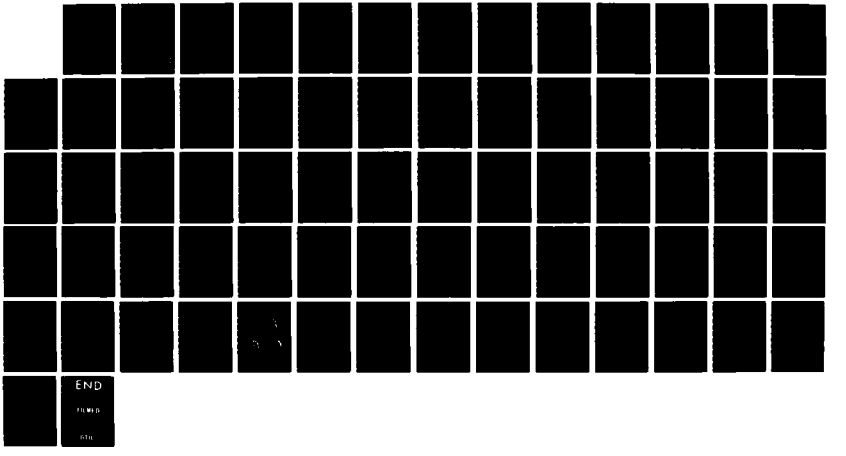

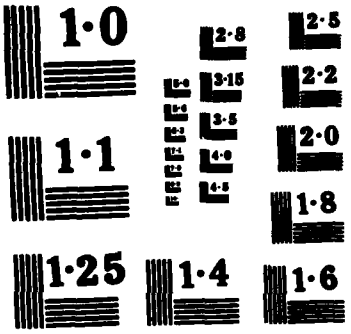

NATIONAL BUREAU OF STANDARDS
MICROCOPY RESOLUTION TEST CHART

2

RADIATION FOG MODELLING

Final Report

September 1982

European Research Office
Contract No DAJA37-81-C-0746

Physics Department
UMIST
Manchester M60 1QD

J Latham
Principal
Investigator

M H Smith
Project
Co-ordinator

S J Perry
Research
Scientist

LIST OF PRINCIPAL SYMBOLS

CC	condensation coefficient
CN	condensation rate
C_p	specific heat of air at constant pressure
D_f	diffusivity of water vapour
e_s	saturation vapour pressure
F_N	net radiative flux
G	graviational sedimentation flux
H	flux of sensible heat
K	turbulent exchange coefficient
k	thermal conductivity of air
LH	latent heat of vaporization
M	molecular weight of water
M_N	mass of nucleii
M_R	mixing ratio
M_{RS}	saturation mixing ratio
N	concentration of droplets
ρ_a	density of air
ρ_L	density of water
Q_a	absorption efficiency of droplets
r	radius of droplet
R_G	universal gas constant
R_N	function of radiative exchange in droplet growth
S	supersaturation
T	dry bulb temperature

W liquid water content

σ surface tension of water vapour

θ potential temperature

Unclassified

SECURITY CLASSIFICATION OF THIS PAGE (When Data Entered)

R&D 4087-R-EN

REPORT DOCUMENTATION PAGE	READ INSTRUCTIONS BEFORE COMPLETING FORM
1. REPORT NUMBER / 2. GOVT ACCESSION NO.	3. RECIPIENT'S CATALOG NUMBER
4. TITLE (and Subtitle) Radiation Fog Modelling	5. TYPE OF REPORT & PERIOD COVERED Final Technical Report Sept.81 - Sept.82 6. PERFORMING ORG. REPORT NUMBER
7. AUTHOR(s) J Latham, M H Smith, SJ Perry	8. CONTRACT OR GRANT NUMBER(s) DAJA37-81-C-0746
9. PERFORMING ORGANIZATION NAME AND ADDRESS Physics Dept. UMIST Manchester M60 1QD England	10. PROGRAM ELEMENT, PROJECT, TASK AREA & WORK UNIT NUMBERS 61102A-1T161102- BH57-01
11. CONTROLLING OFFICE NAME AND ADDRESS USARDSG-UK Box 65, FPO New York NY 09510	12. REPORT DATE September 1982 13. NUMBER OF PAGES 66
14. MONITORING AGENCY NAME & ADDRESS(if different from Controlling Office)	15. SECURITY CLASS. (of this report) Unclassified 15a. DECLASSIFICATION/DOWNGRADING SCHEDULE

16. DISTRIBUTION STATEMENT (of this Report)

Approved for public release; distribution unlimited

17. DISTRIBUTION STATEMENT (of the abstract entered in Block 20, if different from Report)

18. SUPPLEMENTARY NOTES

19. KEY WORDS (Continue on reverse side if necessary and identify by block number)

Radiation fog. Microphysics. Radiative exchanges. Haze. Droplet growth. Supersaturation. Condensation coefficient. Condensation nuclei. Meppen.

20. ABSTRACT (Continue on reverse side if necessary and identify by block number)

In order to further examine the formation and evolution of radiation fogs, a numerical model was developed which contains explicit calculation of the fog microphysics. This model takes into account the evolving micrometeorological characteristics of the boundary layer, which includes the formulation of the radiative exchanges between the overlying atmosphere and the ground, and the subsequent effect of haze development and fully developed fog conditions on these exchanges. In terms of the fog microphysics, the model —

DD FORM 1 JAN 73 1473 EDITION OF 1 NOV 65 IS OBSOLETE

Unclassified

SECURITY CLASSIFICATION OF THIS PAGE (When Data Entered)

20.
accounts for haze development with increasing relative humidity and the effect of radiative loss on the critical supersaturation of the soluble nuclei, in addition to explicitly calculating fog droplet growth.

The resultant model has been tested for the effect of ground conditions on temperature evolution, the effect of the value of the condensation coefficient, and the effect of the nature of the cloud condensation nuclei distribution which is poorly understood at low supersaturations. Brief comparisons have been made with data obtained from the 1980 Meppen field experiment.

INTRODUCTION

Very few studies have been performed concerning the formation of radiation fog through the evolution of the micrometeorological characteristics of the boundary layer and the subsequent interaction between fog microphysics and its continuing development. Early studies were qualitative in nature, and later studies have tended to concentrate only on specific aspects of fog evolution.

A number of the basic mechanisms involved in fog formation were described by Taylor (1917) from routine observations. It was concluded from this study that fogs occurred on occasions of light winds and clear skies, with a pre-existing high relative humidity. It was also suggested that a balance existed between the rate at which air cooled due to the influence of the ground, and the drying of the air by eddy diffusion to ground. If the latter proceeded at a greater rate than the former then fog was unlikely to form.

From observations at Cardington, Stewart (1955, 1957) found that fog formation involved the cooling of the ground by long wave radiation and the subsequent cooling of the air by heat loss through eddy and radiative flux divergence, with radiative cooling as important as turbulent cooling. Stewart also found that, prior to fog formation, the cooling rate increased, which was attributed to radiative heat loss from swelling haze droplets.

Although early studies indicated that radiative exchanges in the lower atmosphere were an essential feature of fog develop-

ment, few detailed studies have been made. In a comprehensive series of field experiments, with wind speeds in the region of 0.5 - 1.0m s^{-1} Funk (1960, 1962) found the radiative flux divergence in the lowest 10m of the atmosphere produced cooling rates of around 3k h^{-1} before fog onset, although greatly increased cooling rates (in the region of 30k h^{-1}) existed for short periods. The cooling rates derived from flux divergence were compared with measured cooling rates, which were often lower, thereby implying a convergence of the sensible heat flux. Funk concluded from this observation that, during occasions of light winds, nocturnal cooling was caused by radiative exchange and not by sensible heat loss to the colder ground. Radiative flux divergence was also found to increase just before fog formation, which was again attributed to the influence of swelling haze nuclei. However, Zdunkowski, Henderson and Hales (1966) contested this proposition utilizing a numerical model which suggested that, even with greatly increased haze concentration, radiative flux divergence would be little affected. Funk also observed that fog could either form in direct contact with the ground, or just above the ground if flux divergence maximised in this region, in which case a layer structure to the fog would then ensue.

The study by Roach et al (1976), to date the most comprehensive reported in the literature, presented the detailed evolution of fog in terms of the micrometeorology. The major findings were:

1. Fog development was closely related to periods of strong cooling associated with small values of wind velocity and,

consequently, turbulence. The major cooling was attributed to radiative exchange, which was offset by convergence of the sensible heat flux when wind velocities were above 1-2m s^{-1}.

2. As the fog continued to develop and grow in height, the surface based inversion was replaced by an adiabatic or superadiabatic lapse. This temperature profile transformation resulted from the increased optical path length reducing the net radiative loss at the ground below the value of the upward soil heat flux. From this stage it was suggested that the fog top would assume, radiatively, the role previously taken by the ground.

3. Although turbulence probes were used, only estimates of the exchange coefficient were made, which yielded values of between $5 \times 10^{-3} m^2 s^{-1}$ to $1\ m^2 s^{-1}$. There were also indications that gravity waves existed in the stable boundary layer.

4. The measured value of liquid water content was found to be considerably smaller than that estimated from cooling rates and resultant condensation. The difference was attributed to the effects of gravitational sedimentation and eddy diffusion to ground. As turbulence on many occasions was limited, gravitational sedimentation was likely to have been the dominant agent.

5. Measurements of the microphysical properties revealed that droplet radii reached a maximum of around 12μm, with a secondary peak in the distribution between 5-10μm. This was found to correspond to the concentration of cloud condensation nuclei at 0.8% supersaturation.

Although Roach et al presented some information concerning

the fog microphysics in relation to the micrometeorology, other microphysical studies have basically failed to undertake detailed measurements of the evolving nocturnal boundary layer, consequently making interpretation of the results in terms of complete fog evolution difficult.

Fairly extensive microphysical measurements were made by Pilie et al (1975) at Elmira, New York State. Cloud condensation nuclei measurements indicated concentrations in the region of $1000cm^{-3}$ at 0.3% supersaturation, with concentrations of haze nuclei declining as the fog developed. For the droplet spectrum at the ground the maximum radius extended to 24μm, with total droplet concentration around $100-200cm^{-3}$. Measurements in the vertical indicated that the droplet spectra narrowed with height. Comparisons of shallow and deep fogs were made in which the maximum supersaturation was greater in the shallow fog but droplet spectra were narrower which was attributed to gravitational sedimentation. Although micrometeorological measurements were made, comparisons with other radiation fogs are difficult to make as mesoscale dynamics induced by the valley were likely to play a significant role.

Low (1975) also established the existence of large drops of around 20μm radius in a radiation fog, with a calculated maximum supersaturation of 0.05% and a liquid water content of $0.2g\ m^{-3}$. The existence of large drops in radiation fogs is contested by Roach et al (1976) who report maximum drop radii in the region of 10μm, a view supported by recent studies at Meppen, West Germany, in which maximum drop radii of around 10 to 12μm were measured at the 2m level. However, earlier studies at Meppen by Choularton

et al (1981) found drops in excess of 20um radius which were associated with periodic high values of mean radius and liquid water content. These periodic fluctuations with their associated large drops, were attributed to convective motions arising in the fog due to strong radiative cooling at the fog top. Although such cooling could lead to enhanced drop growth, it was considered inadequate to explain the existence of the largest drops observed. It was argued that such growth could be a consequence of either fluctuations in supersaturation produced by mixing at the fog top or by the vertical circulation and hence statistically-favoured growth of some drops. Little information is available relating to the form of the droplet spectra with increasing height. In contrast to Pilie et al (1975), Pinnick et al (1978) at Grafenwohr found the concentration of drops in the size range between 4 and 16μm increase with altitude (Figure 1). Consequently the liquid water content (and extinction coefficient) also increased with height, with values at 160m of between 0.2 and 0.8 g m^{-3}. These findings are in accord with the theory of strong radiative cooling at the fog top. Brown (1980) however disagrees, finding maximum droplet radius and extinction coefficient decreasing with height. However, Brown emphasised that his findings related to fogs which may have been influenced strongly by mixing at the fog top. It was found that the creation of a superadiabatic lapse led to convective motions and, subsequently, to a region of maximum wind shear at the fog top. This wind shear may have induced mixing across the interface with consequent evaporation of drops near the upper boundary.

The more recent studies at Meppen lend support to this hypothesis (in contrast to the earlier findings of Choularton et al) by indicating that fluctuations in drop concentration, mean radius and liquid water content were associated with lower values of these quantities. However, lack of data prevents the origin of these effects being unequivocally linked to mixing at the fog top.

NUMERICAL MODELS OF RADIATION FOG

A number of attempts have been made to model accurately the evolution of fog with varying degrees of success. These previous models are reviewed in order to highlight the physical processes which must be simulated in a comprehensive fog model. The results of these earlier models will be discussed in relation to the development of the fog model which is the subject of this report.

Zdunkowski and collaborators have been responsible for several investigations of the evolution of the boundary layer prior to fog formation and to the fog formation process itself. As previously mentioned, Zdunkowski, Henderson and Hales (1966) investigated the effect of haze on radiative cooling rates in the lower atmosphere and concluded that haze had little influence on cooling rates, directly contrasting Funks (1960, 1962) hypothesis that haze accounted for the anomalous flux divergence. Their model predicted that maximum radiative cooling, in the region of $6k\ h^{-1}$, existed at a height of 20cm, with radiative heating existing above to a height of 130cm. They also included a temperature discontinuity of $-3^{o}K$ at the ground which produced radiative cooling rates of around $20h^{-1}$ through the lower boundary layer. A fog model was developed from this work (Zdunkowski and Nielsen 1969), but many aspects of fog evolution were simplified. The turbulent exchange coefficient was a function only of height and did not evolve with time. The only radiative agents were water vapour and water droplets and gravitational sedimentation was not included. Explicit microphysics were not included in the

model - the droplet distribution being derived from the value of the liquid water content. Although the model simulated basic fog formation, the fog grew too rapidly compared with observation, reaching heights in excess of 100m one hour after initiation.

An improved model was reported by Zdunkowski and Barr (1972) which included a more comprehensive treatment of the exchange coefficient taking account of the thermal stability effects (albeit in a fairly crude manner) and also the nature and magnitude of the wind components. The effect of linking the exchange coefficient with the evolving temperature regime increased the time taken for fog formation compared with the earlier model. In many cases shallow ground fog formed approximately 4 hours after sunset and reached 100 metres 7 hours after initiation and gave reasonable liquid water content values (of the order of 0.3g m^{-3}) Furthermore, the model predicted the evolving exchange coefficient in a realistic manner, giving a decrease in the magnitude of the exchange coefficient and in the height of the maximum value as the boundary layer evolved towards fog formation, with the reverse of this sequence after fog formation.

Lala, Mandel and Juisto (1975) evaluated the variables in numerical models of radiation fog, finding that dew formation and the height of the maximum value of the exchange coefficient were the main factors influencing whether or not fog would form. The ensuing model, however, did not account for the radiative influence of the droplets or their gravitational sedimentation, therefore limiting its usefulness.

The fog model presented by Brown and Roach (1976) was partially based on the previous models of Zdunkowski and co-

workers. Although, as in previous models, the explicit calculation of the microphysics was not included, provision was made for gravitational sedimentation. The model was also recalculated with a number of different profiles of the exchange coefficient, some of which were related to thermal stability. Fog formation at the ground occurred between 45 and 75 minutes after initiation, depending on the value of the exchange coefficient. It was found that greater degrees of turbulence enhanced the diffusion of water vapour to the ground and these hindered the formation of fog. The time taken for fog formation was considerably shorter than that found by Zdunkowski and Barr, probably due largely to a higher initial value of the relative humidity. In the evolution of the boundary layer prior to fog formation, the authors stressed the importance of the radiative cooling of the air to the colder ground. The inclusion of gravitational sedimenation was also investigated and was found to produce a lowering of the liquid water content from over 1g kg^{-1} to around 0.3g kg^{-1}. This lowering of liquid water content led, in turn, to a reduced cooling rate by the droplets thereby resulting in a further decrease in condensation and droplet growth.

The UMIST fog model was based upon that of Brown and Roach, extended to include the exact formulation of the microphysics following Brown (1980). The growth equation employed in the model included a term to account for the effect of net radiative loss on droplet growth which leads to a lowering of the critical supersaturation of soluble nuclei. The model accounted for the main features of fog evolution, predicting maximum droplet radius

of around 12μm, and the formation of a superadiabatic lapse below fog top. However, the model was based on a constant exchange coefficient profile with time, and consequently did not take account of thermal development.

Radiation Fog Model

The model, at present, makes use of the following equations to describe the changes in temperature, supersaturation, and liquid water content. An equation to explicitly calculate droplet growth is also included.

Droplet growth.

$$\frac{\delta r}{\delta t} = \left(\frac{1}{A + (AA \times E)}\right)\left[\frac{S}{r} - \frac{B}{r^2} + \frac{CM_N}{r^4} - DR_N Q_a(r)\right] \qquad (1)$$

where

$$A = \frac{L_H \rho_L}{kT}\left(\frac{L_H M}{R_G T} - 1\right)$$

$$AA = \frac{\rho_L R_G T}{D_f M e_s(T)}$$

$$B = \frac{2\sigma M}{\rho_L R_G T}$$

$$C = 6.9246 \times 10^{-5} m^3 kg^{-1}$$

$$D = \frac{1}{kT}\left(\frac{L_H M}{R_G T} - 1\right)$$

$$E = 1 + \left(\frac{\sqrt{\frac{2\pi M}{R_G T}}\, D_f / CC}{r}\right)$$

$$R_N = \frac{1}{2}(F\uparrow + F\downarrow)S_{BC}$$

The first term on the right of equation (1) expresses the effect of the diffusion of water vapour and heat on droplet growth. The expression for the diffusion of vapour includes the condensation coefficient which has a marked influence on droplet growth. The term B in the equation takes into account the effect of curvature and expresses the increase in saturation ratio over a droplet compared to a plane surface. The term C is the solution effect and takes into account the reduction in vapour pressure due to the presence of the salt. The influence of both the curvature and solution terms diminish as the radius of the droplet increases. The final term on the right of equation (1) takes into account the effect of radiative exchange on droplet growth, as discussed by Roach (1976, 1978) and Barkstrom (1978). Generally, as the droplets grow so their influence becomes more marked on radiative transfer in the lower boundary layer, until the cooling rate is dominated by their influence. The principal heat sink is then transferred to the droplets, which become cooler than their environment and consequently depress the saturation vapour pressure over the droplets. An enhanced growth rate is then induced which allows droplets formed on large nuclei to grow in slightly undersaturated air by lowering their critical supersaturation and increasing their equilibrium radii. The relationship between critical supersaturation and radiative loss for several nucleus masses is illustrated in Table 1. Clearly, an increase in radiative loss feeds back to droplet concentration by reducing the peak supersaturation and, hence, the number of droplets activated in the fog.

TABLE 1

Mass (g)	Dry radius (μm)	Critical supersat. ratio % ($0.0 Wm^{-2}$)	Critical supersat. ratio % ($-15 Wm^{-2}$)	Critical supersat. ratio % ($-25 Wm^{-2}$)	Critical supersat. ratio % ($-35 Wm^{-2}$)
8×10^{-15}	0.1	6.8×10^{-2}	6.7×10^{-2}	6.6×10^{-2}	6.6×10^{-2}
1.1×10^{-13}	0.25	1.8×10^{-2}	1.0×10^{-2}	1.1×10^{-3}	5.8×10^{-3}
1.0×10^{-12}	0.53	5.8×10^{-3}	-2.4×10^{-2}	-4.4×10^{-2}	-6.3×10^{-2}
4.1×10^{-12}	0.83	3.0×10^{-3}	-5.6×10^{-2}	-9.5×10^{-2}	-1.3×10^{-1}

Haze droplets and equilibrium radius

From the usual form of the cloud condensation spectra:

$$N = C_{CCN} S^k$$

where N = concentration of nuclei

C_{CCN} = concentration of nuclei activated at 1% supersaturation

S = supersaturation

k = slope of best-fit line

a nuclei distribution of the form

$$\frac{dN}{d\log R} = {}^{K}C_{CCN} R_S^{\,k} \ln 10 R^{-k}$$

may be derived where R = critical radius of the droplet

R_S = a temperature dependent parameter derived from the relationship between critical radius ($\sqrt{3C_{MS}}/B$) and critical supersaturation ($\sqrt{4B^3/27C}$) where B and C have been given and $_{MS}$ is the mass of the salt nuclei.

The concentration and appropriate dry radius, nucleus mass, critical radius and critical supersaturation of a number of different classes of the cloud condensation nuclei distribution may be derived from this equation.

When the relative humidity of a layer exceeds 95%, the

equilibrium radii of the haze droplets are derived from a cubic solution of equation (1) at the appropriate relative humidity and net radiation. These equilibrium radii provide upper limits to the growth of the droplets in any time step, unless a drop has been activated in which case it may exceed its critical radius. Between 95% and 99% relative humidity droplets responds almost instantaneously to any change in humidity and, therefore, the equilibrium radius is taken as the droplet size until the relative humidity exceeds 99%, when the growth equation is fully employed. The upper limit of growth continues to be set at the equilibrium radius as, for small drops, dr/dt becomes large for the time steps employed in the model and consequently can produce numerical instability. Reducing the time step to around 0.1sec would involve an excessive amount of computer time and the error involved by limiting a growing droplet to its maximum equilibrium size, at a particular relative humidity, is small. This restriction only applies during the early stages of droplet growth. As the droplet continues to grow its actual size begins to lag behind the equilibrium size until activation occurs, the extent of this lag being dependent upon the nucleus mass of the droplet.

Temperature evolution

The change in atmospheric temperature is represented by

$$\frac{\delta T}{\delta t} = -\frac{1}{\rho_a C_p}\frac{\delta F_N}{\delta z} + \frac{\delta}{\delta z}\left(K\frac{\delta \theta}{\delta z}\right)\frac{LHC_N}{C_p} \quad (2)$$

The change in temperature is therefore affected by radiative flux divergence, sensible heat flux divergence, and the release of latent heat by condensation. In relation to radiation fog

development, and as turbulence is necessarily small, the major effect on temperature development is through radiative exchange.

The transfer of infra-red radiation in the atmosphere is calculated at each level in the vertical, for five spectral intervals, as given by Rodgers and Walshaw (1966), Partridge and Platt (1976) and Roach and Slingo (1979). The upward and downward fluxes at a particular level, $F_i(z)$ and $F_i(z)$ are given as

$$F_i(z)\uparrow = \left[B_i(grnd) - B_i(z_s)\right] Tr_i(z,z_s) + B_i(z) - \int_{z_s}^{z} Tr_i(z,z') \frac{dB_i(z')}{dz'} \cdot dz' \qquad (3)$$

$$F_i(z)\downarrow = \left[B_i(top) - B_i(ztop)\right] Tr_i(z,ztop) + B_i(z) + \int_{z}^{z(top)} Tr_i(z,z') \frac{dB_i(z')}{dz'} \cdot dz' \qquad (4)$$

$B_i(z)$ = the Plank function flux representing the temperature at that level

z_s = the lowest level for integration in the atmosphere

ztop = the highest level for integration in the atmosphere

$Tr_i(z,z')$ = transmissivity between levels z and z' which contributes to the overall transmissivity in the band between the level of measurement and the top or bottom of the atmosphere.

The first term on the right of equation (3) is included to account for any temperature discontinuity that may exist between that at the ground and the temperature of the air at the lowest level to which the integration is carried.

The method used to solve the above equation is based upon that given by Roach and Slingo, with a few modifications.

The limits and principal absorbers for the five spectral bands are as follows:

Band	Limits(μm)	Principal absorbers
1	25 -	H_2O
2	17 - 25	H_2O
3	13 - 17	H_2O, CO_2
4	8 - 13	Atmospheric window
5	5 - 8	H_2O

The Planck function flux for each spectral band is given as:

$$B_i(z) = a_i T(z)^{bi}$$

where T(z) is the temperature of the air at that level in K and the values of a and b for each spectral band are:

Band(i)	a_i	b_i
1	8.961×10^{-4}	1.991
2	4.676×10^{-6}	2.906
3	2.637×10^{-8}	3.889
4	6.119×10^{-12}	5.360
5	3.069×10^{-18}	7.844

The calculation of the overall transmissivity involves the multiplication of the individual transmissivity values of each absorber in a given spectral band. For the molecular bands Roach and Slingo used an analytic fit to data from the band model of Hunt and Mattingly (1976) and McClutchley (1973). The function derived was:

$$Tr_i(u) = \frac{u_o}{u_o^n + u^n + Cu}$$

where u is the absorber amount in g cm^{-2} and u_o, n and C are given below:

Band	u_o(g cm^{-2})	n	C
1	2.57×10^{-3}	0.6	1.92
2	1.289×10^{-1}	0.6	0.33
3	3.471	0.6	-
3	2.20×10^{-2}	0.43	-
4	-	-	-
5	6.61×10^{-2}	0.4	-

The extra term, Cu, was required for the calculation of the transmissivity for water vapour in spectral bands 1 and 2 only. To account for the difference between the transmissivity values calculated over zenith angle and parallel radiation, a diffusivity factor of 1.66 (Rodgers and Walshaw) is applied to scale the absorber amount. However, unlike Roach and Slingo the correction for changing atmospheric height and consequently pressure by averaging absorber amount over a given path length is not taken into account due to the relatively small atmospheric depths involved.

The major influence on the transmissivity, however, results from the strong absorption by water droplets, which provides the main mechanism by which fog continues to develop. The transmissivity due to the droplets has the form:

$$Tr_i(z,z') = \exp[-Od(z,z'] \qquad (5)$$

where the optical depth Od(z,z') is obtained by integrating the absorption cross section of the droplets, and is given by:

$$Od(z,z') = 1.66\int_{z}^{z'}\int_{0}^{\infty} N(r,z'')\pi r^2 Q_a(r)\,dr\,dz'' \qquad (6)$$

where N is the concentration of droplets and $Q_a(r)$ is the absorption efficiency of droplet of radius r.

$Q_a(r)$ is given by:

$$Q_a(r) = A_i[1 - \exp(-B_i r)]$$

with A and B taking on the following values for each spectral band:

Band (i)	A_i	B_i
1	-	-
2	1.6	0.25
3	1.35	0.45
4	1.13	0.16
5	1.3	0.1

In band 1 $Q_a(r) = 1.3r$, with $Q_a(r)$ not being allowed to exceed 1.4.

At present the radiation scheme is a simplified version of that given by Roach and Slingo. The scattering effect of droplets is omitted, but the error in the cooling rate has been found to be only between 4% and 9%. The absorption produced by the dimer molecule is also omitted, Partridge and Platt (1976) finding that its main influence is felt in tropical atmospheres.

The net upward longwave radiative flux is then given by:

$$F_{Ni}(z)\uparrow = F_i(z)\uparrow - F_i(z)\downarrow \qquad (7)$$

and the heating rate of the layer by:

$$H(z) = \frac{1}{\rho c_p}\left(\frac{d}{dz}\sum_i F_{Ni}(z)\uparrow\right) \qquad (8)$$

Ground Temperature

The temperature at the ground is calculated following the method employed by Zdunkowski and Nielsen (1969) and Zdunkowski and Trask (1971). The temperature evolution at the ground surface is given by:

$$\frac{\partial Ts}{\partial t} = \frac{\partial}{\partial z}\left(K_s \frac{\partial Ts}{\partial z}\right) \quad z < 0,\ t > 0 \tag{9}$$

where Ts = soil temperature in the topmost layer

Ks = molecular exchange coefficient for soil.

To obtain the change of temperature at the air/ground boundary, Zdunkowski and Nielsen give, in finite difference form:

$$\frac{T_{s,j+1} - T_s}{\Delta t} = \left[\frac{1}{\frac{C_p K \rho_s \Delta Z_s}{K_{s+1} - 3K_s} - \frac{C_s K' \rho_s \Delta Z_s^{-1}}{3K'_s - K'_{s-1}}}\right] \times \left[F_N + \frac{2c_p \rho_s K^2_s}{\Delta Z_s (K_{s+1} - 3K_s)} (T_{s+1} - T_s) - \frac{2C_s \rho_s (K')^2 S}{\Delta Z_{s-1}(3K'_s - K_{s-1})} (T_{s-1} - T_s)\right]$$

where c_p = specific heat of air

K = exchange coefficient of air

K' = molecular exchange coefficient for soil

ρ_a = density of air

C_s = specific heat of soil

ρ_s = density of soil

T = temperature

F_N = net radiative flux

and S refers to the surface and S+1 and S-1 to the layers immediately above and below the surface.

The turbulent exchange coefficient

Given that the flux of sensible heat is given by

$$H = -\rho c_p K_H \delta\theta/\delta z \qquad (10)$$

where K_H is the exchange coefficient for heat and that, on the basis of dimensional theory, Monin and Obukhov (1954) established the flux profile relationship for temperature to be

$$\frac{\delta\theta}{\delta z} = -\frac{H}{\rho c_p k u_* z}\,\phi_H(z/L) \qquad (11)$$

where k = von Karmans constant

u_* = friction velocity

$\phi_H(z/L)$ = universal function from the relationship between z and L, where L is the Obuklov length scale,

then the exchange coefficient, by rearranging and substitution, is given by

$$K_H = k u_* z / \phi_H(z/L) \qquad (12)$$

Under adiabatic conditions, in the absence of buoyancy, $\phi_H(z/L) = 1$, and therefore Ru_*z corresponds to the adiabatic value of the exchange coefficient. Under non-adiabatic conditions this term can be determined from

$$K_H = K_{ad}/\phi_H(z/L) \qquad (13)$$

where K_{ad} = the adiabatic value.

Many forms of the relationship between the universal stability parameter, $\phi(z/L)$, and the Richardson number have been derived, but for the present, the model makes use of that given by Pruitt, Morgan and Lourence (1973), where

$$\phi(z/L) = 0.855(1 + 34Ri)^{0.4} \text{ when } Ri > 0 \qquad (14)$$

$$\phi(z/L) = 0.855(1 - 22Ri)^{-0.4} \text{ when } Ri < 0 \qquad (15)$$

where Ri, the Richardson number, is defined by

$$Ri = \frac{(g/T)(\delta\theta/\delta z)}{(\delta u/\delta z)^2}$$

where g = gravitational velocity

θ = potential temperature

T = temperature

u = wind velocity

Instead of explicitly calculating the wind profile, the model calculates the windshear $\delta u/\delta z$ from the friction velocity, u_*, in the form $\delta u/\delta z = u_*/kz$.

It is also assumed that the exchange coefficient for heat, vapour, and momentum are equal ($K_H = K_w = K_m$).

A more complete discussion of the exchange coefficient in relation to the developing boundary layer will be presented in a later section.

Supersaturation

The change in supersaturation at each time step is given by:

$$\frac{\delta s}{\delta t} = \frac{1}{M_{RS}} \frac{\delta M_R}{\delta t} - \frac{L_H M}{R_G T^2} \frac{\delta T}{\delta t} \qquad (16)$$

The temporal evolution of the supersaturation therefore responds to the change in mixing ratio induced by condensation onto the growing drops and the flux of water, and to the change of temperature.

Liquid water content

The liquid water content is given by

$$\frac{\delta w}{\delta t} = \frac{4}{3}\pi\rho_L \frac{\delta}{\delta t} \sum_i \sum_j N_{ij} r_{ij}^3 \qquad (17)$$

Condensation rate

$$C_N = \frac{\delta w}{\delta t} - \frac{\delta G}{\delta z} - \frac{\delta}{\delta z}\left(K\frac{\delta w}{\delta z}\right) \qquad (18)$$

The degree of condensation is a result of the changing liquid water content, and the amount of flux of water produced by eddy diffusion and gravitational sedimentation.

Mixing ratio

The mixing ratio is simply given by

$$M_R = (1 + S)M_{RS} \qquad (19)$$

and the evolution of the mixing ratio by

$$\frac{\delta M_R}{\delta t} = \frac{\delta}{\delta z}\left(K\frac{\delta M_R}{\delta z}\right) - C_N$$

Numerical Model Results

The radiation fog model is similar to that developed by Brown and Roach (1976) and Brown (1980) though with certain modifications. These models were the first to incorporate detailed microphysics in determining the evolution of fog, although other important aspects, such as turbulence and stability, with their subsequent effects on microphysical development, have been generally left unexplored. Gravitational sedimentation has yet

to be included realistically in the model reported here, which consequently results in enhanced liquid water contents and also rapid fog development after the first 90-120 minutes. This feature of the model will however be discussed more fully in a later section.

Boundary layer evolution

The model was initiated with an isothermal temperature regime of 283K and a constant mixing ratio, resulting in a relative humidity of 95% in the lowest 200m of the boundary layer. The soil was taken to be dry clay with its properties given in Table 2. The friction velocity was taken as 0.1m s^{-1}, corresponding to a mean wind velocity of 1m s^{-1} over relatively smooth terrain. The downward flux of radiation assumed at the top of the model boundary layer at 200m produced a net upward radiative flux at the surface of approximately 70W m^{-2}.

At the initiation of the model, atmospheric cooling results only from direct radiative loss to space, principally through the atmospheric window. This radiative loss is induced by the change in the path length in the lower atmosphere. Variations may be produced, however, if the model is initiated with a non-isothermal temperature structure. The initial cooling rate in the atmosphere is consequently small, in the region of 0.05K h^{-1}, comparable with that given by Brown and Roach. As the ground begins to cool by net longwave radiative loss to space, at a rate of approximately 3K h^{-1}, the air near the surface responds by radiating to the colder ground and thereby increasing its cooling rate. After 15 minutes, the air at the ground-air inter-

face has reached saturation and the cooling rate at 4m has increased to 0.4K h^{-1}. After 45 minutes the cooling rate at 4m has increased to 1K h^{-1}. The air at this height reaches saturation 73 minutes after the initiation of the model after cooling by 1K, by which time the ground has cooled by 3.2K. The temperature evolution in the lower boundary layer is shown in Figure 2.The height of the fog top, which is defined at present by a relative humidity in excess of 97% is also shown.

After saturation at 4m, the fog continues to develop rapidly, with the fog top rising to 30m 1hr and 45 minutes after model initiation. After 2 hours, an adiabatic lapse has developed near the ground. The rapidity of this development is a consequence of the high values of liquid water content in the absence of gravitational sedimentation. In this case, liquid water contents reach 1.2g m^{-3}, a figure in accordance with that given by Brown and Roach when gravitational sedimentation is disregarded. The high water content values, with their associated large drops, increase absorption, especially in the 8-12μm band. Thus, large variations in radiative flux are produced and excessive cooling rates develop leading to adiabatic profile development.

Fog evolution was also calculated with additional radiative exchange as described by the first term in equation 3. This term takes into account the temperature difference between the ground and the top of the vegetation, where Oke (1970) found a temperature minimum. This temperature difference results in enhanced cooling in the lower boundary layer as the air radiates to a surface at a lower temperature. The temperature profile evolu-

tion is shown in Figure 3. After 15 minutes, the cooling at 4m is 1.1K h^{-1} and saturation at this level is reached in 51 minutes compared with 73 minutes in the previous case. Conversely, ground cooling has been lessened due to the reduction in net longwave loss brought about by the more rapid development of high relative humidities and drop growth. As the fog continues to develop and the influence of water drops on radiative exchange increases, the change to an adiabatic lapse in the lower layers occurs approximately 30 minutes earlier.

The influence of soil type on boundary layer evolution and fog development has also been investigated. The soil types used were wet clay, dry and wet sand, and old snow. The properties of these surfaces are given in Table 2. The evolution of the temperature profiles, with and without additional radiative exchange, are shown in Figures 4 to 9, and certain properties of the developing boundary layer in Table 3. With the additional radiation term omitted, the major influence on fog evolution is the moisture content of the soil. The wet soils have greatly enhanced densities, specific heats, heat capacities, conductivities and diffusivities. Therefore they permit a greater absorption of any heat loss or gain with consequently reduced extremes of temperature. In comparison with dry clay, the initial ground cooling rate for wet clay is approximately halved, and saturation at the ground-air interface is reached 15 minutes later. Saturation at 4m is reached in 1 hour and 50 minutes, compared with 1 hour and 13 minutes for dry clay. The same general situation is observed for wet sand. However, despite the increased time taken for fog formation, after saturation, radi-

ative cooling induced by the droplets becomes dominant and again leads to the development of an adiabatic profile in the lower layers of the atmosphere.

The model has also been calculated using an old snow cover and the development of the temperature profile is shown in figs 10 and 11. The initial cooling of the ground is greatly enhanced compared with other soil types leading to saturation at the ground/air interface after only 10 minutes and after 1 hour at 4m. Generally, the fog and an adiabatic lapse developed more rapidly for this case.

The model at present assumes that turbulent heat exchange is relatively insignificant due to the low values of the exchange coefficient. However, the evolution of the turbulence regime, especially in relation to strong stability, is still unclear and consequently the relative roles of radiative and turbulent cooling remain vague. As discussed previously, Funk (1960) found large values of radiative flux divergence near the ground, partially offset by sensible heat convergence. Similar results were found by Rider and Robinson (1951). Measurements of temperature profiles above a variety of surfaces by Oke (1970) show a minimum in temperature at heights up to 50cm. However, Oke could not determine the exact cause of the minimum but postulated that they may have been produced by an elevated haze layer. These results may show that radiative warming was taking place at very low levels thus lending support to the argument put forward in Fleagle and Businger (1963). This concept is further supported by results presented by Schaller (1977), where a combination of

observations and numerical modelling show that radiative warming took place below 20cm, with strong radiative cooling above.

The development of the surface-based inversion and the temperature structure with height (and hence the conditions conducive to fog formation) are consequently a result of the interplay between radiative and turbulent heat exchange at various levels in the atmosphere. André and Mahrt (1982), from experimental and numerical results, found that clear air radiative cooling dominates temperature reductions only when turbulence is almost completely suppressed. However, when turbulence is present, temperature changes in the lower layers of the atmosphere are dominated by the divergence of the sensible heat flux and radiative cooling is only important in the upper layers of the boundary layer. In this case, radiative warming exists in the lowest 10-20m of the atmosphere.

Results obtained by Garratt and Brost (1981) using a second-order closure model to determine nocturnal boundary-layer evolution produce somewhat different results, although comparison between models is difficult to make due to variations in turbulence levels. Near the surface the total cooling rate of approximately 1K h^{-1} was found to be produced principally from radiative flux divergence, partially offset by sensible heat convergence. These results were similar to those produced by Funk. Above this level, the divergence of the sensible heat flux maintained the cooling rate and, at the top of the inversion, the radiational cooling again dominated.

Fog microphysics

As mentioned previously, the development of the fog microphysics is greatly influenced by radiative exchange throughout the evolution of the fog, and in turn the radiative exchange responds to the evolving microphysics. Such exchange at first affects the critical supersaturation of the larger droplets, lowering them in some cases to below zero. For example, in the case of ammonium sulphate $(NH_4)_2SO_4$, values of the critical supersaturation ratio (%) are presented in Table 4 for net radiative loss of 15, 25 and 35W m^{-2}, in comparison with values in the absence of such loss.

The result of this process is that droplets forming on larger salt nuclei have greater equilibrium radii than they would have in the absence of this exchange and they therefore attain and exceed their critical radii at an earlier stage. In some cases droplets may be activated in slightly undersaturated air. Thus the maximum supersaturation and therefore the concentration of activated drops may be reduced in situations where radiative exchange between the droplets and their immediate environment occurs.

As the droplets continue to grow, the level of radiative loss remains a major influence on their growth rate. As it is difficult to distinguish the various influences on the growth rate of a population of droplets (and also to allow comparison with previous investigations), the effect of net radiative loss was isolated from other factors influencing the microphysical evolution. In all the following cases the droplet radius was

taken to be 4μm at t=0. Figures 12 and 13 illustrate the effect of radiative loss on droplet growth with a variety of nucleus masses and a constant supersaturation. Without radiative loss droplets grow to between 14 and 17μm in 50 minutes depending on the masses of the original nuclei. With a radiative loss of 30W m^{-2}, droplets grow to between 23μm and 26μm in the same duration. Radiative exchange consequently greatly enhances drop growth although, in reality, droplets are unlikely to experience this degree of radiative exchange for such a duration. Figures 14 and 15 illustrate the effect of radiative exchange on droplet growth with a constant supersaturation of 0.0% and 0.05%. In the absence of radiative loss, and with zero supersaturation, droplet growth is severely restricted, with growth from 4μm to 7μm in 50 minutes. However, a similar droplet experiencing radiative loss of 30W m^{-2} would grow to 16μm over the same period. With a constant supersaturation of 0.05%, droplets experience growth with and without radiative exchange, although radiative exchange clearly leads to enhanced growth.

Although gravitational sedimentation is not at present included in the microphysical evolution of the model fog, an approximate method of determining its effect was included in the simplified model described above. The gravitational velocity was described by:

$$V_T = \frac{2r^2 g(\rho w - \rho a)}{9\eta}$$

where ρw = density of water

ρa = density of air

g = acceleration of gravity

η = dynamic viscosity of air

r = droplet radius

which is applicable to droplets of less than 40μm. A profile of the net upward longwave radiative flux which had a maximum value of 30W m^{-2} at 30m, and decreased with decreasing height was also included in the calculations. The combined effect of droplet growth with radiative exchange and gravitational sedimentation is shown in Figure 16, with a constant supersaturation throughout the 30m depth of the atmosphere of 0.05%. Initially the droplet growth is enhanced by the influence of the radiative exchange but, as the droplet settles through the fog, this exchange decreases and the rate of growth consequently decreases. For a nucleus mass of 1×10^{-11}gms the droplet takes 24 minutes to reach the ground at which time its radius has increased to 16μm. For a droplet with nucleus mass of 1×10^{-12}gms the time taken to reach the ground increases to 32 minutes and the maximum radius decreases to 14μm. When the supersaturation was set to zero (Figure 17) throughout the 30m of atmosphere the maximum radius attained by the droplet with nucleus mass of 1×10^{-11}gms was 14μm and 9μm for a nucleus mass of 1×10^{-12}gms.

Although the calculations adopted here are only a simplified version of the processes taking place in a radiation fog, the results indicated that the maximum radius which can occur in a fog under the influence of sedimentation is in the region of 16μm, depending on the depth of fall and the magnitude of the radiative exchange. The prediction of the maximum radius is therefore dependent on the knowledge of the net upward radiative flux profile and the degree of turbulence which may act to oppose

the sedimentation of droplets.

The complete radiation fog model was originally formulated with a cloud condensation nuclei distribution of the form:

$$N = 1500S^{0.5}$$

which is typical for continental air masses as defined by previous investigators (Pruppacher and Klett, 1978). The nuclei were assumed to be completely soluble ammonium sulphate, $(NH_4)_2SO_4$. This form of the CCN distribution produced a total concentration of nuclei of $340cm^{-3}$ with a critical supersaturation below 0.07%, and a total mass of $132\mu g\ m^{-3}$. Although gravitational sedimentation was not included, the initial development of the droplet spectrum appears to be realistic. In respect of the night-time boundary layer evolution over a dry clay soil, the development of the droplet spectrum, including the haze phase, from the initial dry nuclei is shown in Figure 18. Also displayed is the critical radius corresponding to each class of nucleus. As the ground-based inversion develops, the CCN respond immediately, at first, to the increasing relative humidity although, subsequently, the droplets formed from larger nuclei, with their relatively slow response times, lag behind their equilibrium sizes. Consequently, the larger nuclei are never activated. However, the dimensions of intermediate-sized nuclei increase beyond their critical sizes and droplets are activated, as can be seen from the figure. The low values of supersaturation found in the fog are insufficient to activate the three smallest classes of nuclei. After 1 hour and 45 minutes, the maximum droplet radius at 4m is 15.5μm although, with sediment-

ation this would most probably be reduced. The maximum supersaturation attained at this level is 0.038%, a figure which agrees with that found by previous investigators.

The development of the droplet size distribution in the boundary layer influenced by a wet clay soil (Figure 19) clearly reveals the influence of the reduced cooling rate. The droplet spectrum develops more slowly, the maximum supersaturation attained is lower at 0.023% and fewer classes of nuclei are activated.

It can be seen that the form of the CCN distribution and the effect of gravitational sedimentation play an important role in the development of the fog microphysics. The CCN distribution utilized provides a high concentration of large nuclei which, as grown drops, remain in the distribution. Even though the larger droplets may not be activated, the lowering of their critical supersaturation by radiative exchange below that present in the fog, causes them to continue to absorb available water. Therefore, they tend to decrease the supersaturation and the number of droplets activated. Conversely, the high concentration of large droplets in the fog have a pronounced effect on radiative flux divergence and cooling, and therefore assist in maintaining the level of supersaturation. If sedimentation was included, the concentration of large droplets and the liquid water content would decrease to more realistic levels, in turn leading to reduced cooling rates.

Fog condensation nuclei

Recently there has been discussion in the literature as to

the exact form of the condensation nuclei distribution at low supersaturation. The previous analyses were based on a distribution that is widely reported to represent continental air masses and has been used in previous investigations of fog microphysics. Although the actual concentration of nuclei at low supersaturations are not measured by the commonly-used, Mee CCN counter, it was believed that the activation curve could be interpolated to lower levels. However, Hoppel (1979), Hudson (1980) and more recently Alofs and Liu (1981) have produced results using diffusion cloud chambers which allow the measurements of activated nuclei over a wider range of supersaturation. Alofs and Liu show that, in the range of 0.681% to 0.013% supersaturation, there are two distinct activation curves, with the change in slope occurring around 0.05% supersaturation.

Because of the importance of the nuclei distribution in the initial development of the drop size spectrum, the results obtained by Alofs and Liu were incorporated into the model. Between 0.07 and 0.05% supersaturation the nuclei distribution was represented by the form:

$$N = 3000S^{0.4}$$

and for the remainder of the distribution by:

$$N = 4 \times 10^{6}S^{3.0}.$$

Utilizing these formulae gives a total nuclei number concentration of $620cm^{-3}$ and a total mass of $22\mu g\ m^{-3}$.

The resultant drop size spectrum at a height of 4m for a boundary layer influenced by a dry clay soil is shown in Figure 20, representing a liquid water content of $0.19g\ m^{-3}$. The con-

centration of droplets greater than 1μm is 530cm^{-3}. For comparison, a spectrum is included from the Meppen 1980 experiment for approximately the same water content with a droplet concentration of 590cm^{-3}.

The effect of a variation in the condensation coefficient

The fog evolution model was also formulated with a variation in the value of the condensation coefficient. In the cases presented above, the coefficient was set at a value of 3.3 x 10^{-2}, a value used by Brown (1980). By reducing the coefficient to 3.3 x 10^{-3} a significant effect on the spectrum is observed (Figure 21 and Figure 22). In both cases the lower value of the condensation coefficient reduces the growth rate, increases the maximum supersaturation, and allows the activation of the smaller droplets. Consequently the spectrum becomes narrower, the maximum radius being reduced from 10-11μm to 7-8μm as more droplets compete for the available water and the growth rate is slowed.

Conclusion

Although the model still requires the inclusion of gravitational sedimentation, the major processes contributing to the pre-fog and early fog structure are realistically simulated. The development of the model has emphasised the importance of the radiative exchange on the temperature evolution in the boundary layer and also on the development of the droplet spectrum, with its associated feedback to the radiation budget. However, the relative roles of radiative exchange and sensible heat exchange are not adequately understood at present, and further numerical investigation is required to enable the model to closely examine the development of the nocturnal boundary layer under a variety of conditions. The model was also formulated to represent a variety of initial condensation nuclei distributions because of the importance of the form of the activation spectrum at the low values of supersaturation often found in fogs. In this way, the model predicted that the form of the initial nuclei distribution can affect the ensuing droplet spectrum and that droplet spectra similar to those obtained during the Meppen 1980 experiment can be produced.

Apart from gravitational sedimentation which is currently being incorporated, the fog model requires additional processes which are not presently included in any existing model to be taken into account for the complete simulation of fog. The development of the droplet spectrum, and its related transmissivity and visibility, require the inclusion of the effects of convective motions beneath the fog top, the effect of horizontal wind

shear and its significance at low wind velocities and the effect of gravity waves and other extreme stability phenomena. All of these processes may produce entrainment and mixing of air masses of varying histories within the fog and subsequently affect the nature of the droplet spectrum with height and the further development of the fog. With such a wide range of reported maximum sizes and droplet concentrations in fogs, all existing models are inadequate in the descriptions of these important features.

REFERENCES

Alofs D J and Liu T-H 1981 Atmospheric measurements of CCN in the supersaturation range 0.013-0.681%. J Atmos Sci, 38,2772-2778

André J C and Mahrt L 1982 The nocturnal surface inversion and influence of clear air radiative cooling. ibid,39, 864-878

Barkstrom B R 1978 Some effects of the 8-12um radiant energy transfer on the mass and heat budgets of cloud droplets. ibid,35, 665-673

Brown R and Roach W T 1976 The physics of radiation fog:II- a numerical study. Quart J Roy Met Soc,102,335-354

Brown R 1980 Some field observations of radiation fog and their interpretation. VIII Int Conf Cloud Phys, Clermont-Ferrand,p309-312

1980 A numerical study of radiation fog with an explicit formulation of the microphysics. Quart J Roy Met Soc, 106,781-802

Choularton T W Fullarton G, Latham J, Mill C S, Smith M H and Stromberg I M 1978 A field study of radiation fog in Meppen, West Germany. ibid,107,381-394

Fleagle R G and Businger J A 1963 An introduction to atmospheric physics. Academic Press

Funk J P 1960 Measured radiative flux divergence near the ground at night. Quart J Roy Met Soc,86, 382-389

1962 Radiative flux divergence in radiation fog. ibid,88,233-249

Garratt J R and Brost R A 1981 Radiative cooling effects within and above the nocturnal boundary layer. J Atmos Sci, 38,2730-2746

Hoppel W A 1979 Measurement of the size distribution and CCN supersaturation spectrum of submicron aerosols over the ocean. ibid, 2000-2015

Hudson J 1980 Relationship between fog condensation nuclei and fog microstructure. ibid, 37,1854-1867

Hunt G E and Mattingly 1976 Infrared radiative transfer in planetary atmospheres. I.Effects of computational and spectroscopic economies on thermal heating/cooling rates. J Quant.Spectrosc.Radiat. Transfer,16,505-520

Lala G G, Mandel E and Jiusto J E 1975 A numerical evaluation of radiation fog variables. J Atmos Sci,32,720-728

Low R D H 1975 Microphysical evolution of fog. J Rech Atmos 2,23-32

McClatchey R A, Benedict W S Clough S A, Burch D E, Calfee R F, Fox K, Rothman I S and Goring J S 1973 AFCRL Atmospheric absorption line parameters compilation. Environmental research paper, No.434

Monin A S and Obukhov A M 1954 The basic laws of turbulent mixing in the surface layer of the atmosphere. Akad.Nauk. SSSR Trud.Geofiz.Inst.,No.24(151),163-187

Oke T R 1970 The temperature profile near the ground on calm nights. Quart J Roy Met Soc.,96, 14-23

Paltridge G E and Platt C M R 1976 Radiative processes in meteorology and climatology. Developments in Atmospheric Science,5. Elsevier.

Pilie R J, Mack E J, Kocmond W C, Eadie W J and Rogers C W 1975 The life cycle of valley fog. PtII:Fog microphysics. J Appl Met,14,364-374

Pinnick R G, Hoihjelle D L, Fernandez G, Stenmark E B, Lindberg J D, Hoidale G B, and Jennings S G 1978 Vertical structure in atmospheric fog and haze and its effects on visible and infrared extinction. J Atmos Sci,35,2020-2032

Pruitt W D, Morgan D L, and Lourence F J 1973 Momentum and mass transfers in the surface boundary layer. Quart J Roy Met Soc, 99, 370-386

Pruppacher H R and Klett D 1980 Microphysics of Clouds and Precipitation. Reidel

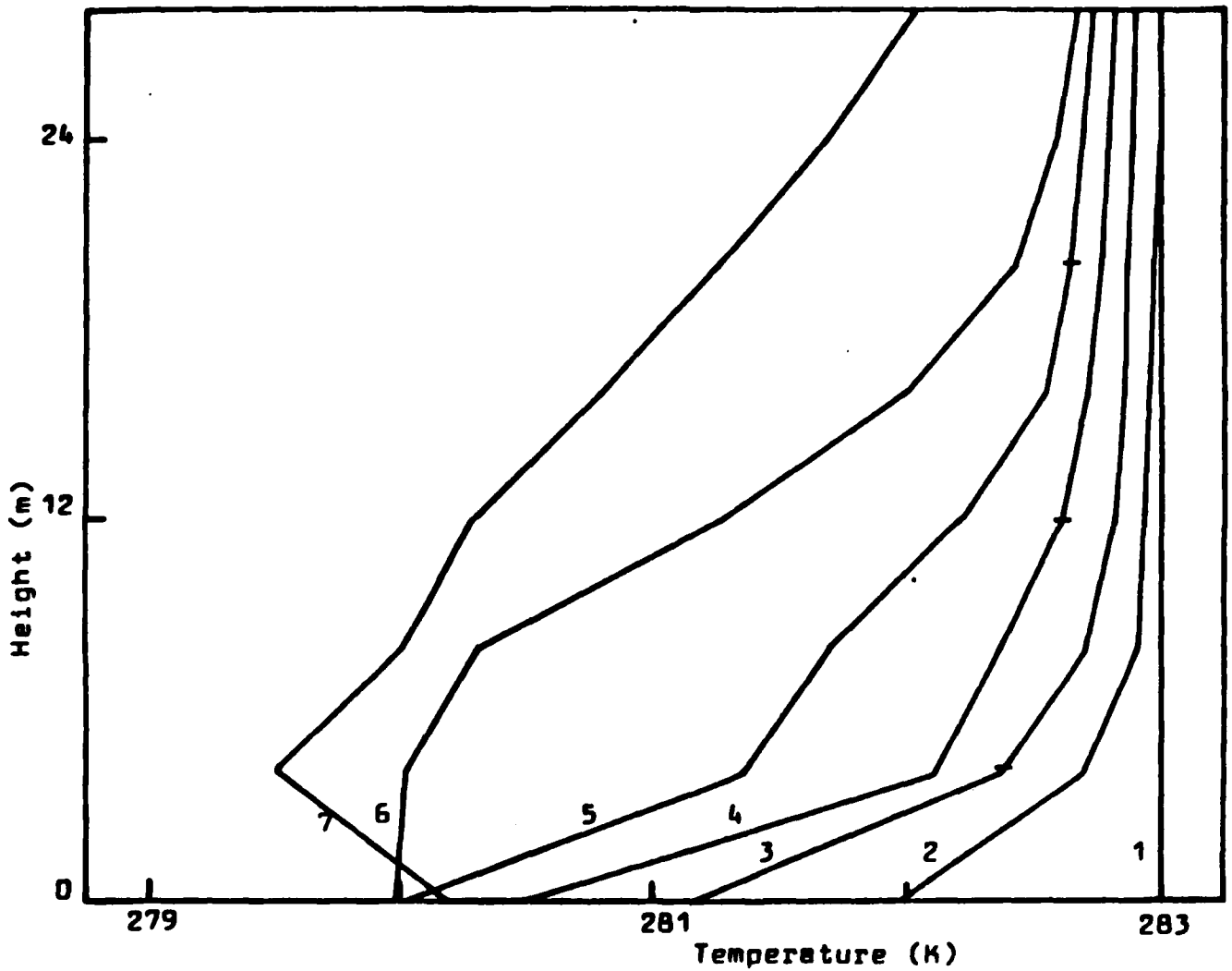

Figure 11: Temperature evolution in the boundary layer over an old snow cover, including the effect of a vegetation minimum in temperature, with an initial isothermal atmosphere of 283K.

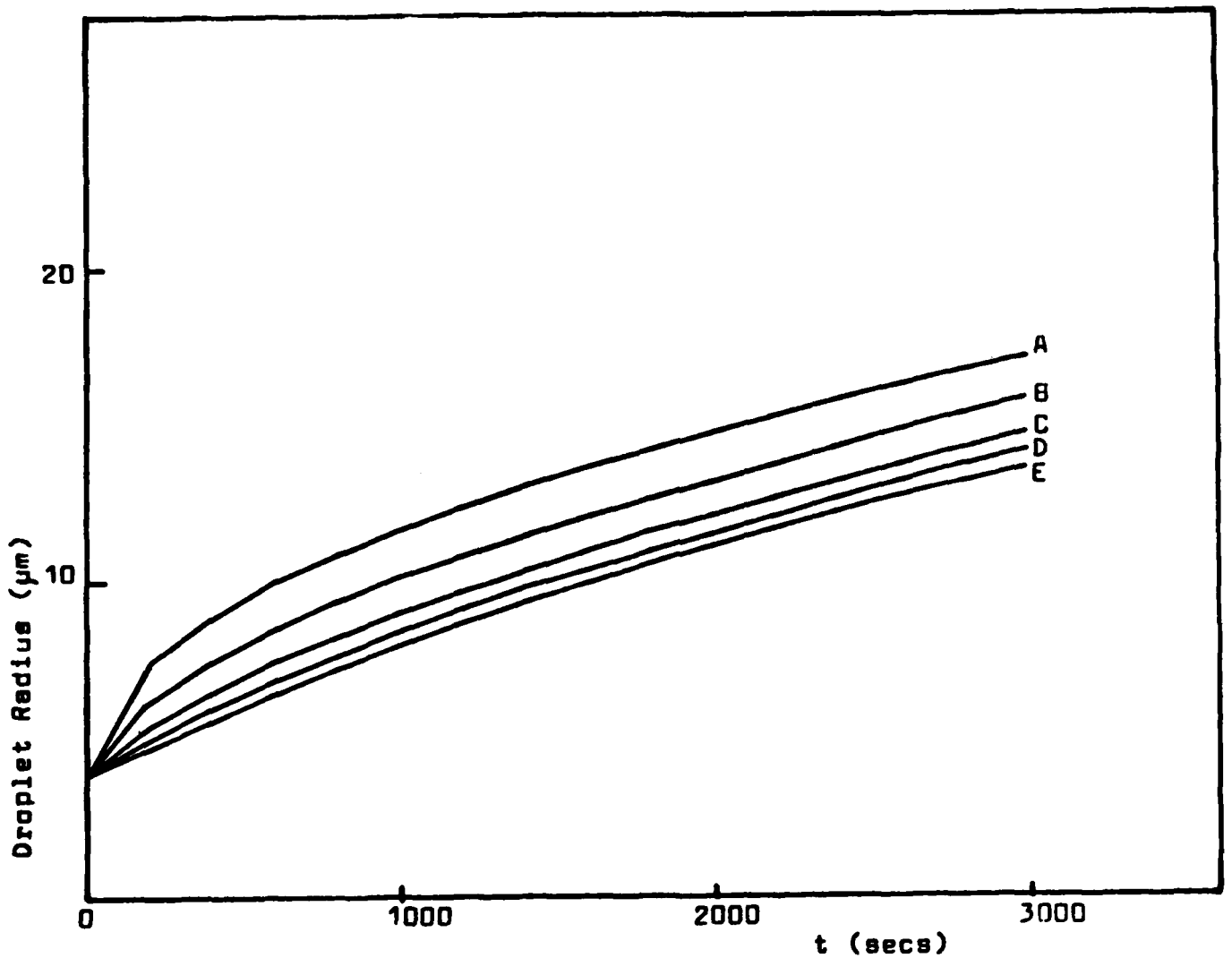

Figure 12: Droplet growth from an initial radius of 4μm with nucleus masses of 3×10^{-12}gms(A), 1×10^{-12}gms(B), 3×10^{-13}gms(C), 1×10^{-13}gms(D), 3×10^{-14}gms(E), without radiative exchange and with a constant supersaturation of 0.05%

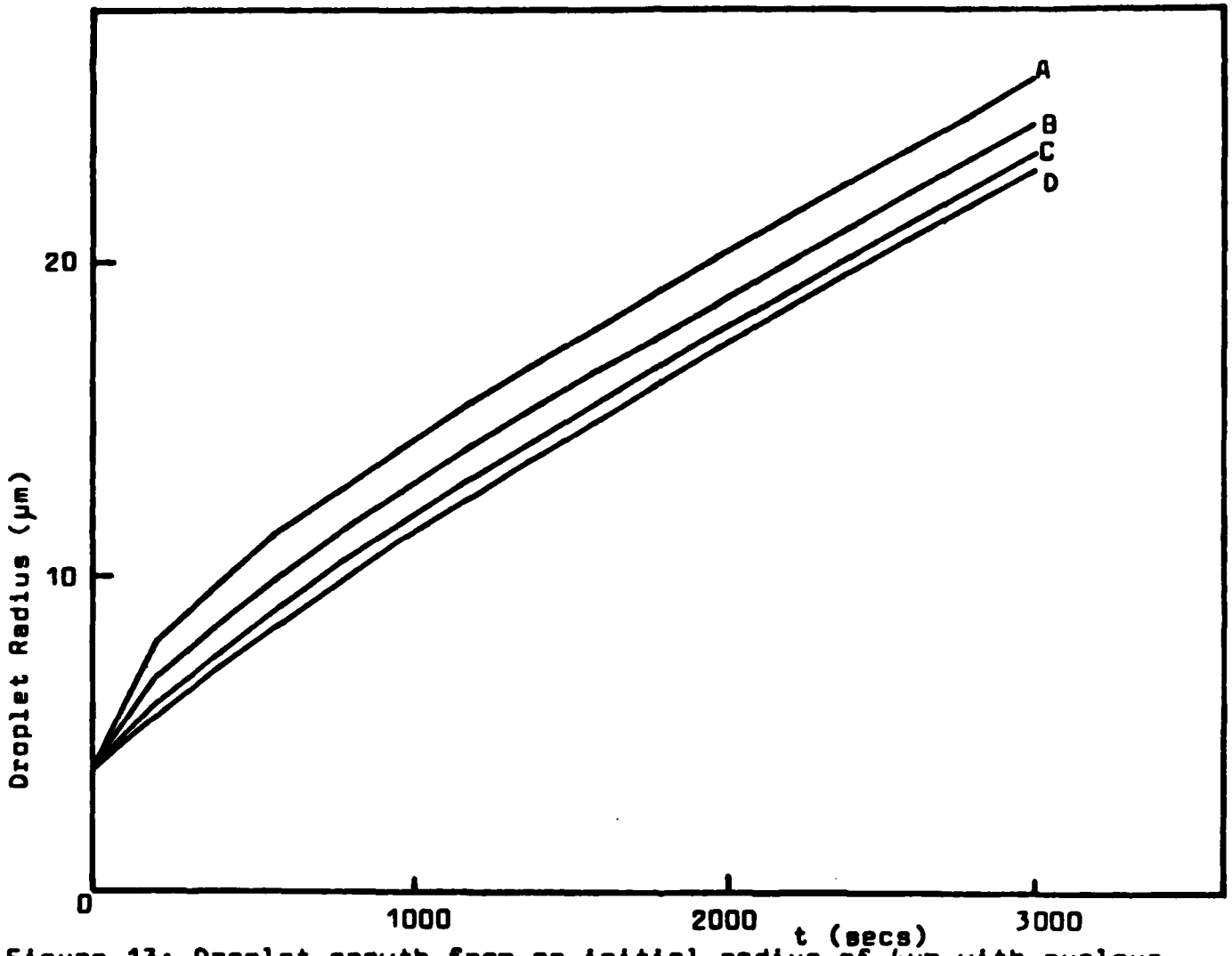

Figure 13: Droplet growth from an initial radius of 4μm with nucleus masses of 3×10^{-12}gms(A), 1×10^{-12}gms(B), 3×10^{-13}gms(C), 1×10^{-13}gms(D), with a net radiative loss of 30W m^{-2} and a constant supersaturation of 0.05%

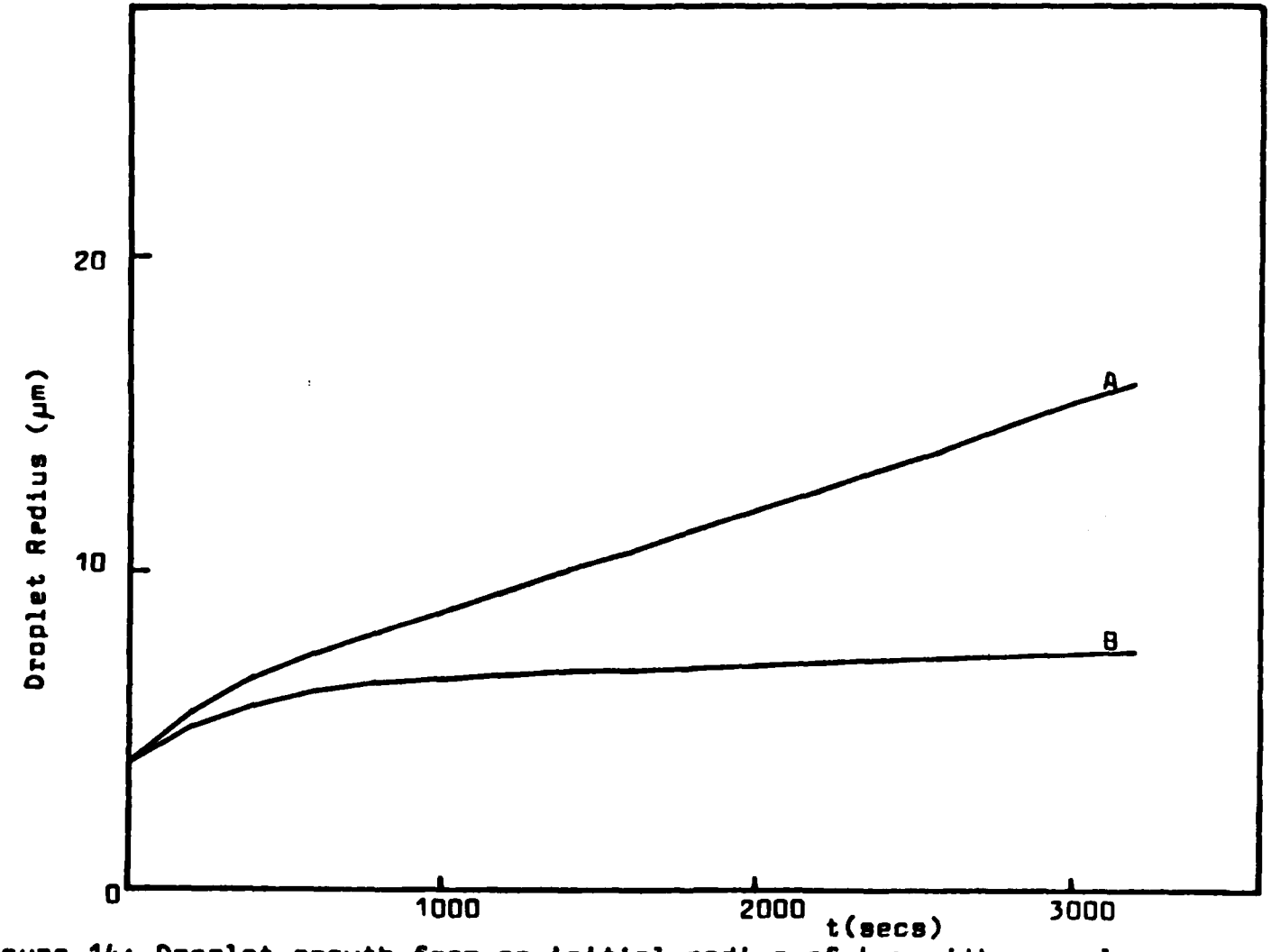

Figure 14: Droplet growth from an initial radius of 4μm with a nucleus mass of 1 x 10^{-12}gms and a zero supersaturation with a net radiative loss of 30W m^{-2}(A) and zero radiative loss (B)

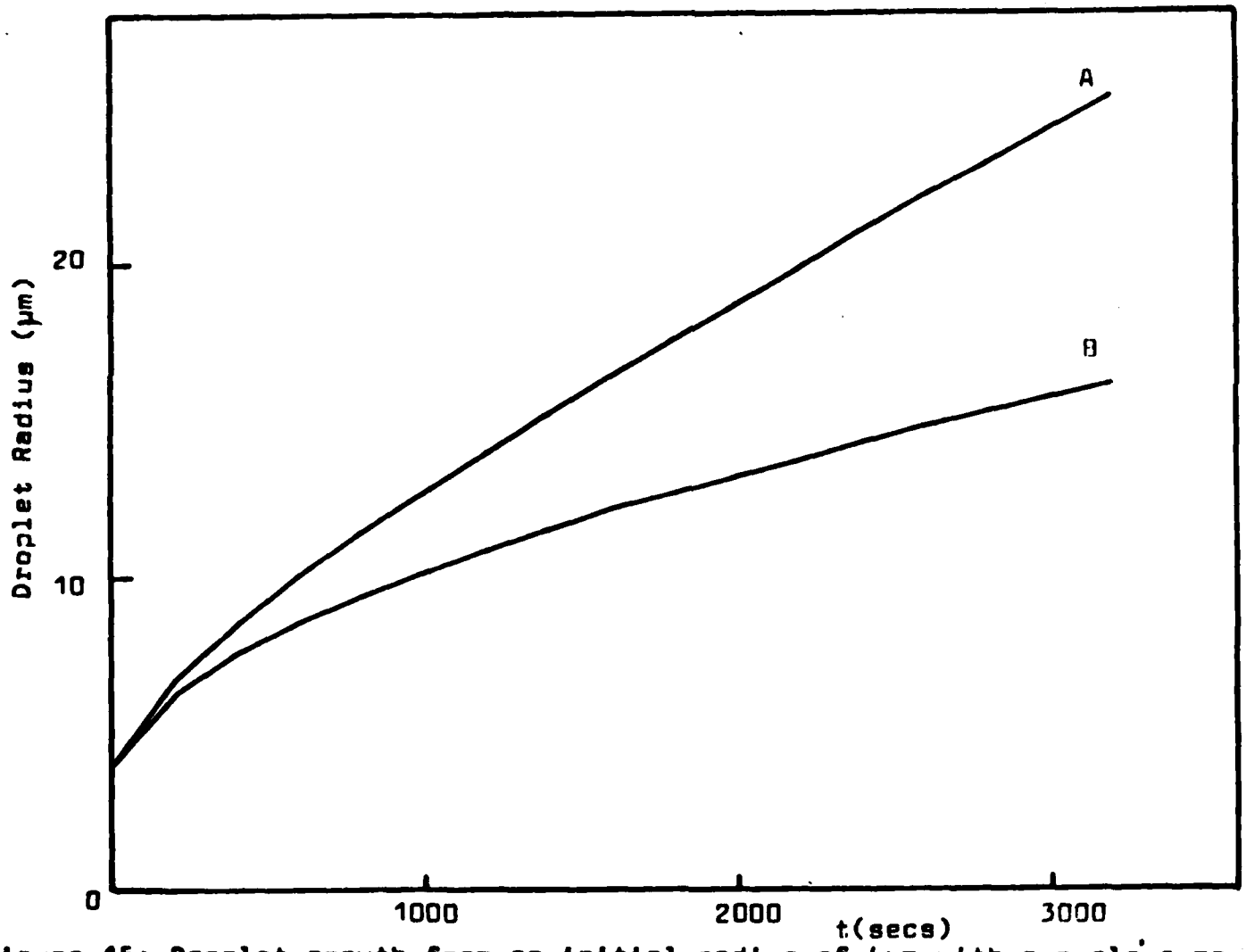

Figure 15: Droplet growth from an initial radius of 4μm with a nucleus mass of 1×10^{-12}gms and a constant supersaturation of 0.05% with a net radiative loss of 30W m^{-2}(A) and with zero radiative loss (B)

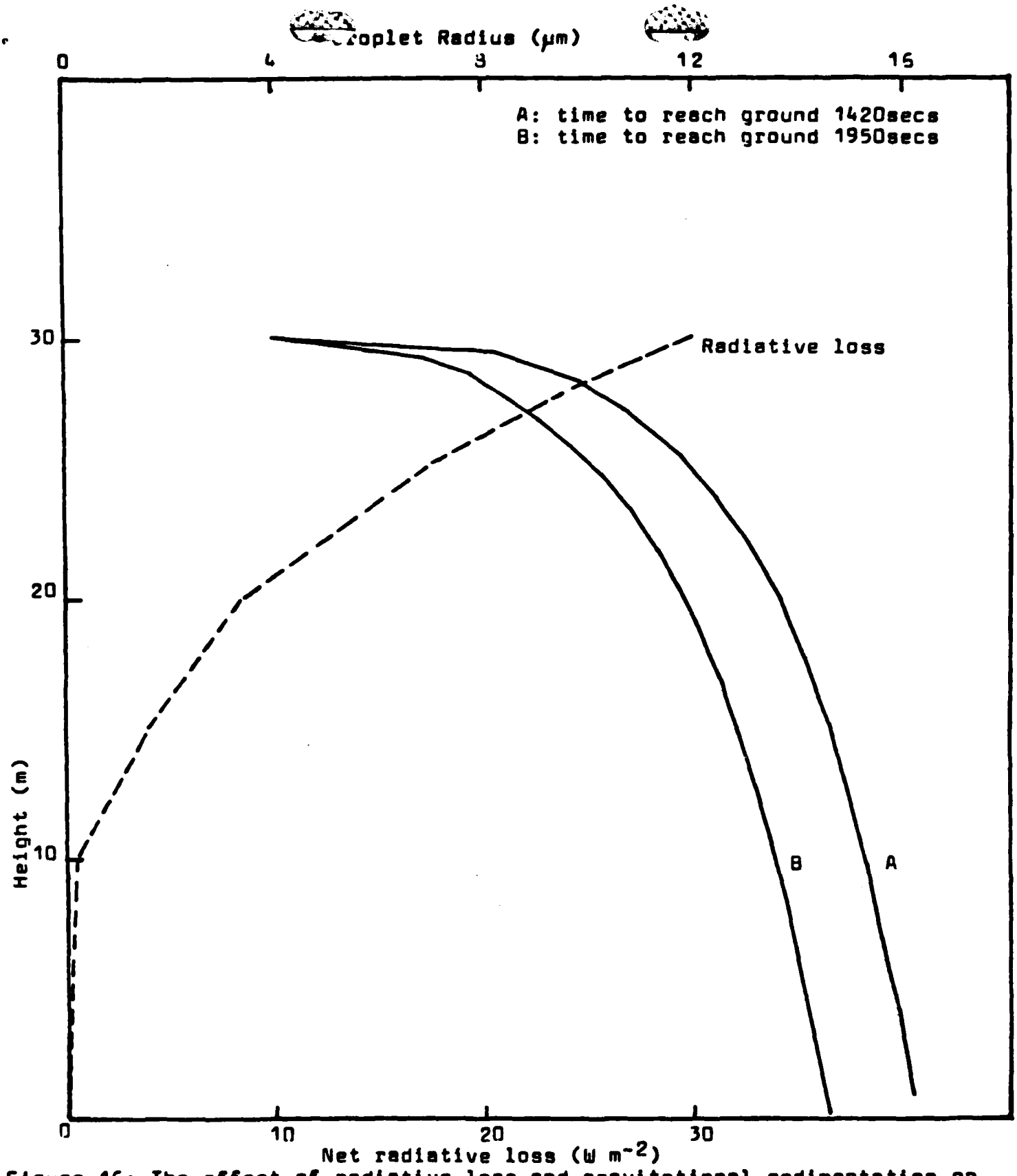

Figure 16: The effect of radiative loss and gravitational sedimentation on a droplet of initial radius 4um and nucleus mass 1 x 10^{-11}gms (A) and 1 x 10^{-12}gms (B) falling from 30m through fog with a constant super-saturation of 0.05%

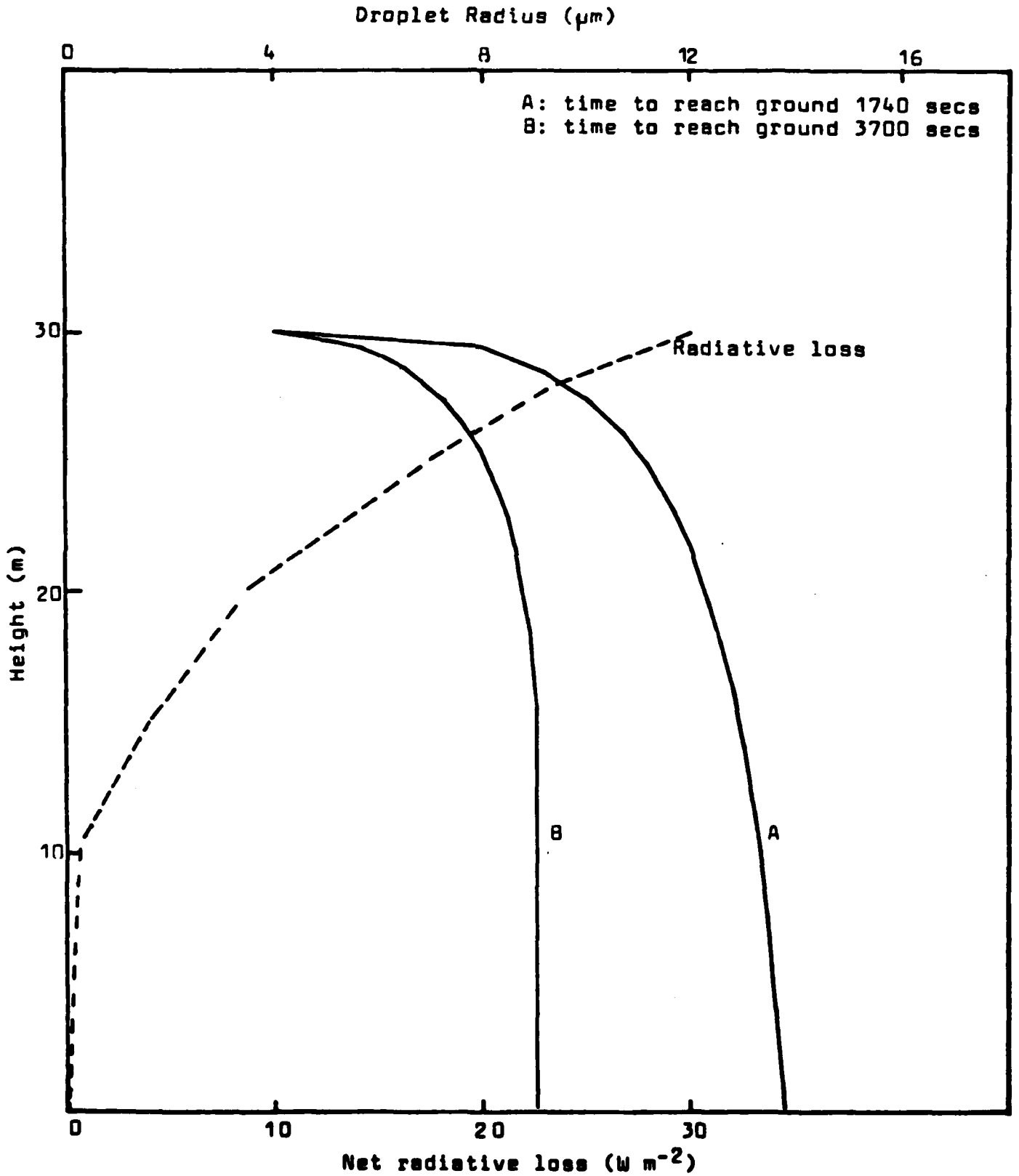

Figure 17: The effect of radiative loss and gravitational sedimentation on a droplet of initial radius 4μm and nucleus mass 1 x 10^{-11}gms (A) and 1 x 10^{-12}gms (B) falling from 30m through fog with zero supersaturation

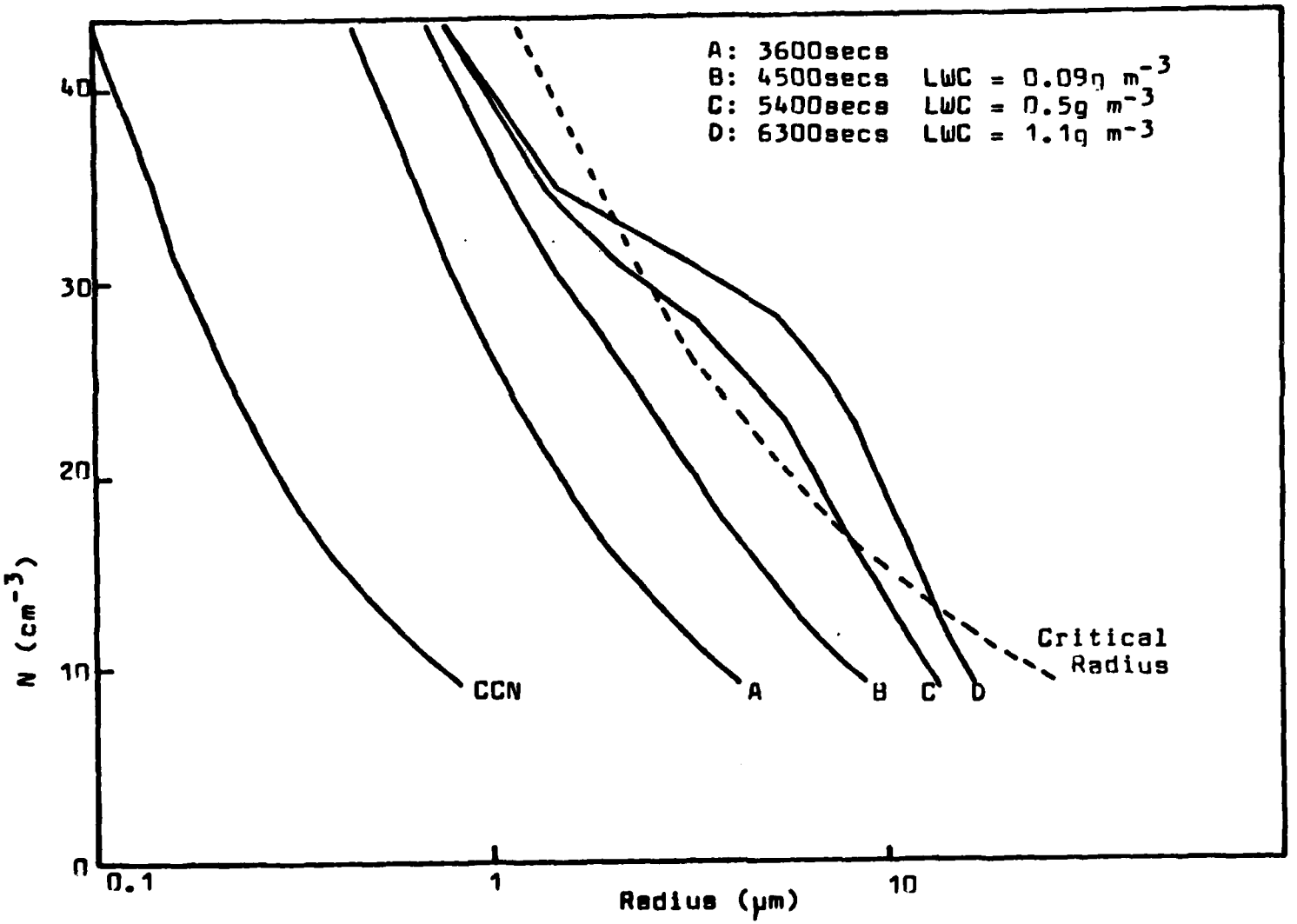

Figure 18: Temporal evolution of the droplet distribution at 4m over a dry clay soil from the initial CCN distribution

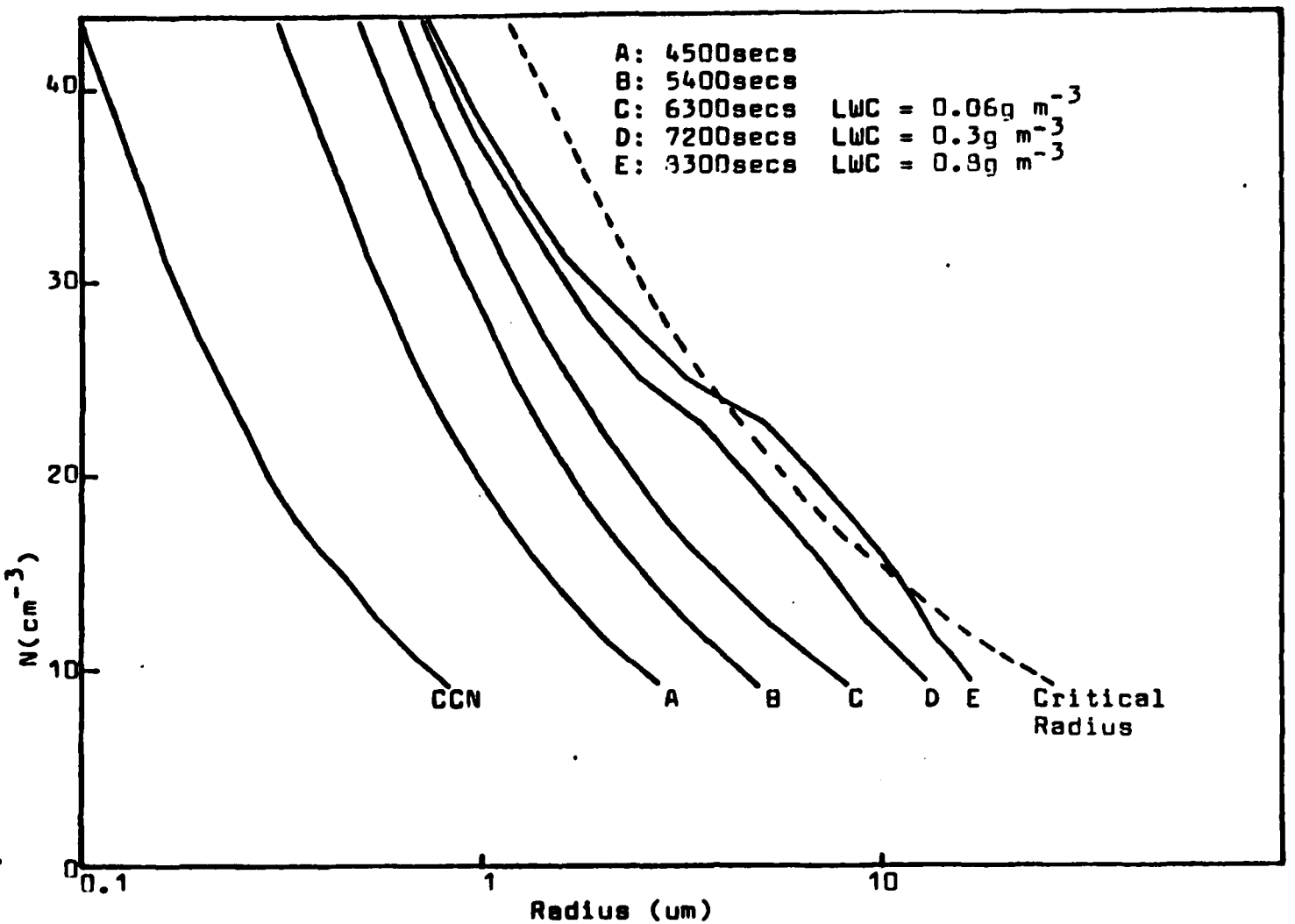

Figure 19: Temporal evolution of the droplet distribution at 4m over a wet clay soil from the initial CCN distribution

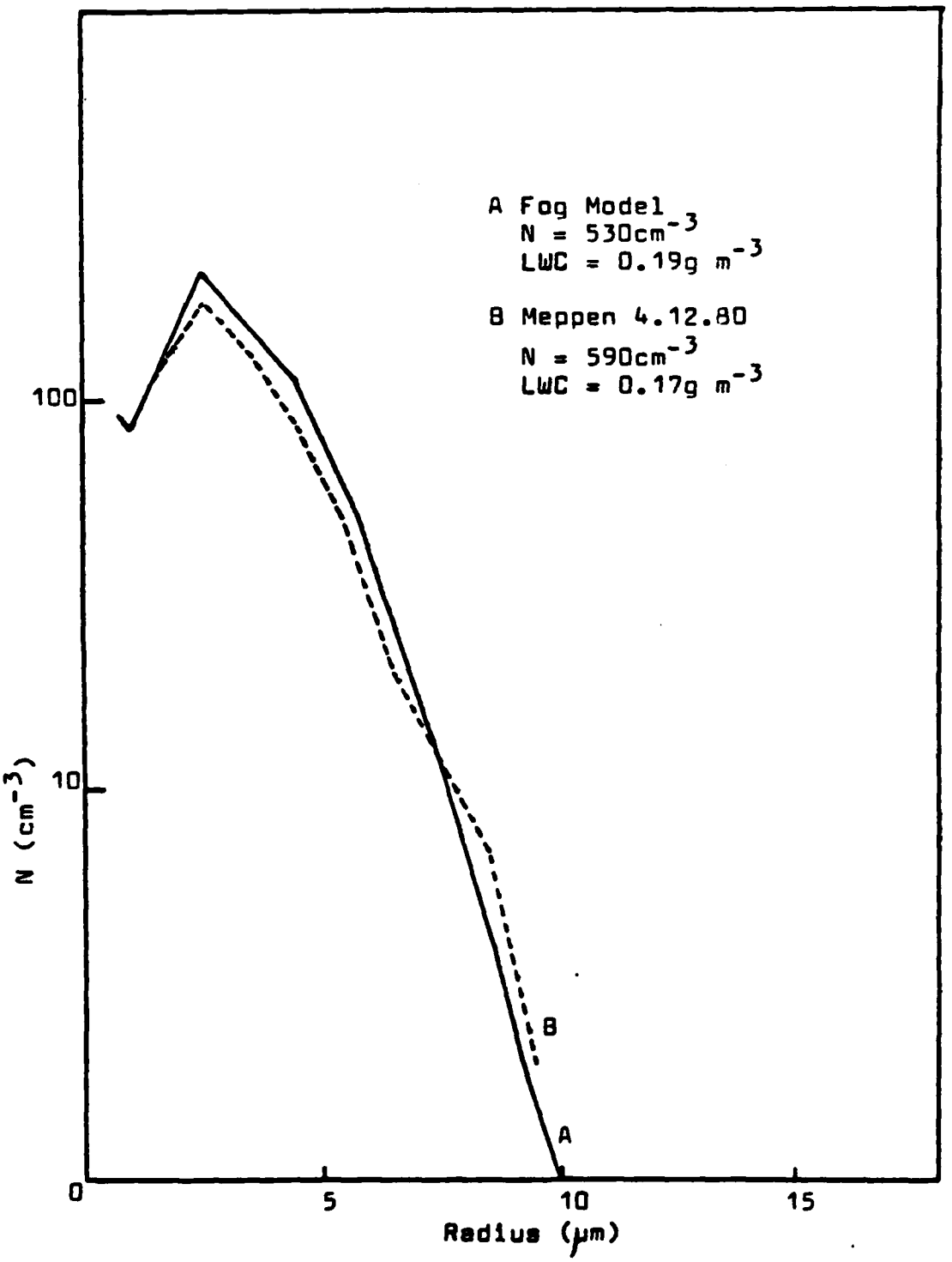

Figure 20: Comparison of the droplet distribution from the fog model with droplet distribution obtained from Meppen

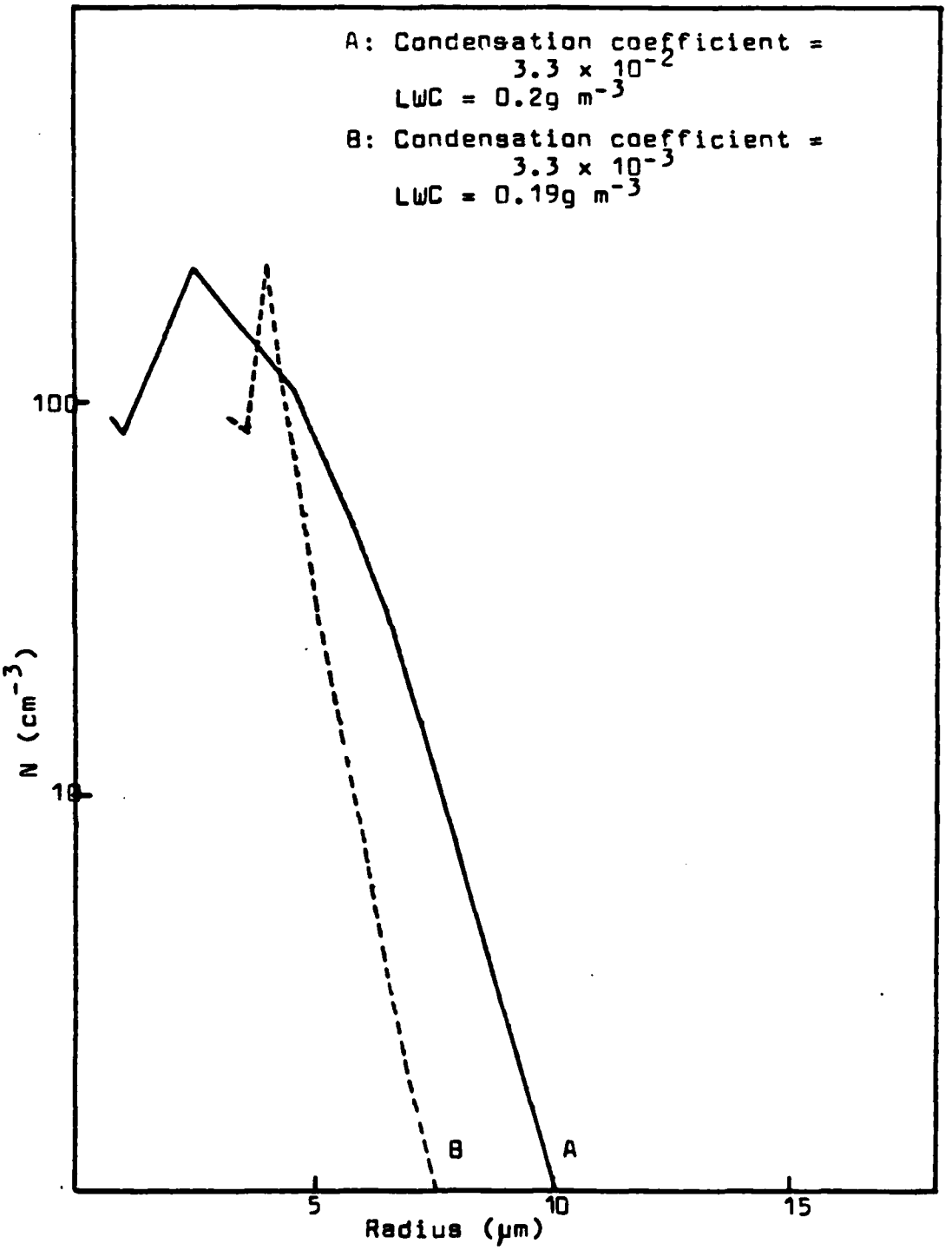

Figure 21: The effect of the condensation coefficient on the droplet distribution at 4m over a dry clay soil

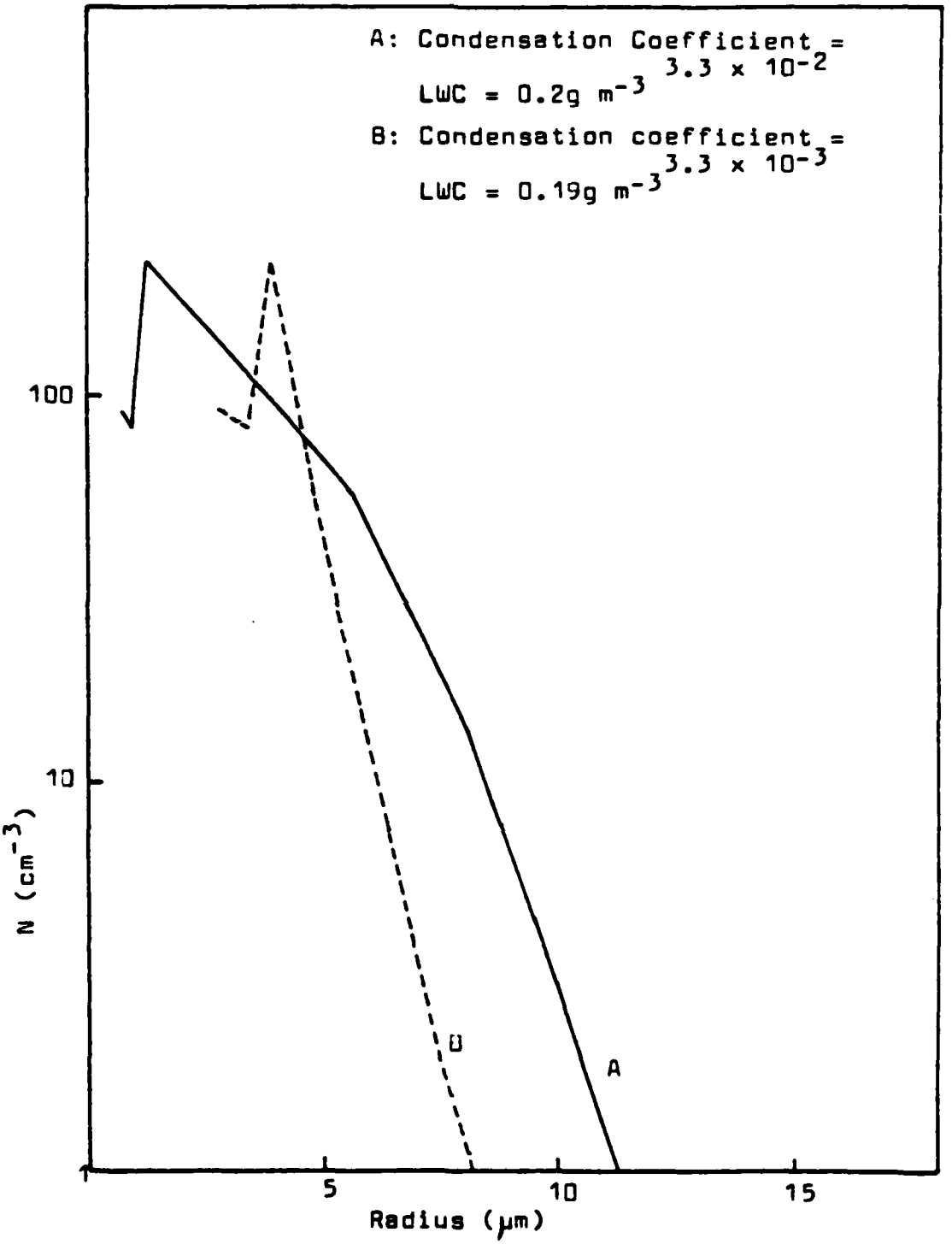

Figure 22: The effect of the condensation coefficient on the droplet distribution at 4m over a wet clay soil

Rider N E and Robinson G D 1951 A study of the transfer of heat and water vapour above a surface of short grass. Quart J Roy Met Soc.,77,375-401

Roach W T 1978 On the effect of radiative exchange on the growth by condensation of a cloud or fog droplet. ibid, 102,361-372

1978 Radiative transfer and cloud droplet growth. J Atmos Sci,36,372-373

Roach W T, Brown R, Caughey S J, Garland J A and Readings C J 1976 The physics of radiation fog:I - a field study. Quart J Roy Met Soc, 102,313-333

Roach W T, and Slingo A 1979 A high resolution infrared radiative transfer scheme to study the interaction of radiation with cloud. ibid, 105,603-614

Rodgers C D and Walshaw C D 1966 The computation of infrared cooling rate in planetary atmospheres. ibid, 92,67-92

Schaller E 1977 Time and height variability of the sensible heat flux in the surface layer. B.L.Met.,11, 329-354

Stewart K H 1955 Radiation fog:investigations at Cardington 1951-54.Air Ministry. Met Res paper 912.

1957 Some observations on the composition of fog. Air Ministry, Met Res paper 1074.

Taylor G I 1917 The formation of fog and mists. Quart J Roy Met Soc.,43,241-268

Zdunknowski W and Barr A E 1972 A radiative conductive model for the prediction of radiation fog. B.L.Met.,2,152-177

Zdunkowski W, Henderson D and Hales J V 1966 The effect of atmopsheric haze on infrared radiative cooling rates. J Atmos Sci.,23,297-304

Zdunkowski W and Nielsen B C 1969 A preliminary prediction analysis of radiation fog. Pure & Appl Geoph,75,278-299

Zdunkowski W and Trask D C 1971 Application of a radiative-conductive model to the simulation of nocturnal temperature changes over different soil types. J Appl Met,10,937-948

TABLE 2
SOIL PROPERTIES

	Density ($kg\ m^{-3} \times 10^{3}$)	Specific heat ($J\ kg^{-1}K^{-1} \times 10^{3}$)	Heat Capacity ($J\ m^{-3}K^{-1} \times 10^{6}$)	Thermal conductivity ($W\ m^{-1}K^{-1}$)	Diffusivity ($m^{2}s^{-1} \times 10^{-6}$)
Dry Sandy soil	1.6	0.8	1.28	0.3	0.24
Wet Sandy Soil	2.0	1.48	2.96	2.2	0.74
Dry Clay	1.6	0.89	1.42	0.25	0.18
Wet Clay	2.0	1.55	3.10	1.58	0.51
Old Snow	0.48	2.09	0.84	0.42	0.40

TABLE 3

Soil Type	Initial Cooling Rate at Ground (K)	Initial Cooling Rate at 4m (K)	Saturation at Ground (secs)	Cooling Rate at 4m after 900secs (K)	Time for R.H. to increase from 99-100% (secs)	Saturation at 4m (secs)	Cooling Rate at 4m at Saturation (K)
1	3	0.05	900	0.40	1160	4400	1.6
2	3	0.83	1000	1.1	1140	3080	1.6
3	1.4	0.02	1800	0.20	1900	6620	1.7
4	1.4	0.80	2120	0.92	1920	4200	1.9
5	3.4	0.05	800	0.44	1080	4160	1.7
6	3.4	0.84	900	1.1	1080	2960	1.7
7	1.5	0.02	1700	0.20	1780	6400	1.7
8	1.5	0.80	2020	0.93	1840	4100	1.9
9	4.3	0.06	600	0.55	940	3680	1.7
10	4.3	0.84	700	1.2	940	2700	1.9

Temperature Profile Types

1 Dry Clay
2 Dry Clay (Grass Minimum)
3 Wet Clay
4 Wet Clay (Grass Minimum)
5 Dry Sand
6 Dry Sand (Grass Minimum)
7 Wet Sand
8 Wet Sand (Grass Minimum)
9 Old Snow
10 Old Snow (Grass Minimum)

TABLE 4

Mass (g)	Dry Radius (μm)	Critical Supersat. Ratio(%) (0.0W m^{-2})	Critical Supersat. Ratio(%) (-15W m^{-2})	Critical Supersat. Ratio(%) (-25W m^{-2})	Critical Supersat. Ratio(%) (-35W m^{-2})
8×10^{-15}	0.1	6.8×10^{-2}	6.7×10^{-2}	6.6×10^{-2}	6.6×10^{-2}
1.2×10^{-13}	0.25	1.8×10^{-2}	1.0×10^{-2}	1.1×10^{-3}	5.8×10^{-3}
1.0×10^{-12}	0.53	5.8×10^{-3}	-2.4×10^{-2}	-4.4×10^{-2}	-6.3×10^{-2}
4.1×10^{-12}	0.83	3.0×10^{-3}	-5.6×10^{-2}	-9.5×10^{-2}	-1.3×10^{-1}

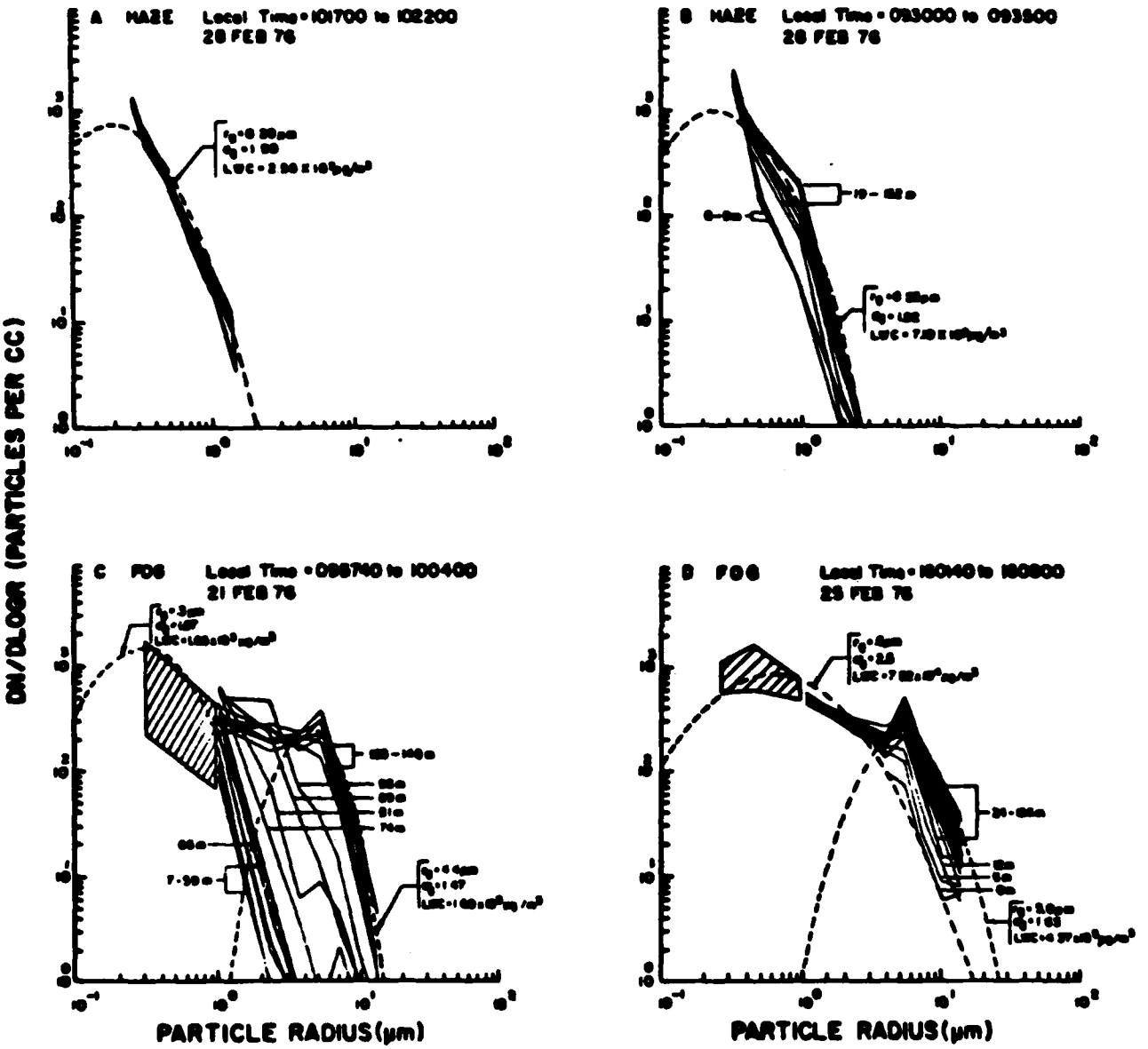

FIG. 6. Particulate size distribution measurements made near Grafenwöhr, West Germany, with a tethered balloonborne aerosol counter for several haze and fog conditions. Each size distribution is for a particular altitude or altitude range as indicated. Measurements at particular altitudes (121 m in Fig. 6a, 95 m in Fig. 6b, 59 and 126 m in Fig. 6c, and ground level and 135 m in Fig. 6d) have been fitted with log normal size distributions (dashed curves) for the purpose of estimating the effects of extrapolating the measured distributions. Values of geometric mean radius r_g, geometric standard deviation σ_g and liquid water content LWC are shown with the corresponding log-normal curves. The date, local time (hours, minutes, seconds) and time interval for the measurements are given.

Figure 1: Droplet size distribution variation with height in haze and fog (as Fig 6 of Pinnick et al 1978)

Figures 2 - 11

Temperature Curve Descriptions

Curve	Time After Fog Initiation (Mins)
1	0
2	15
3	30
4	45
5	60
6	75
7	90
8	105
9	120
10	135
11	150

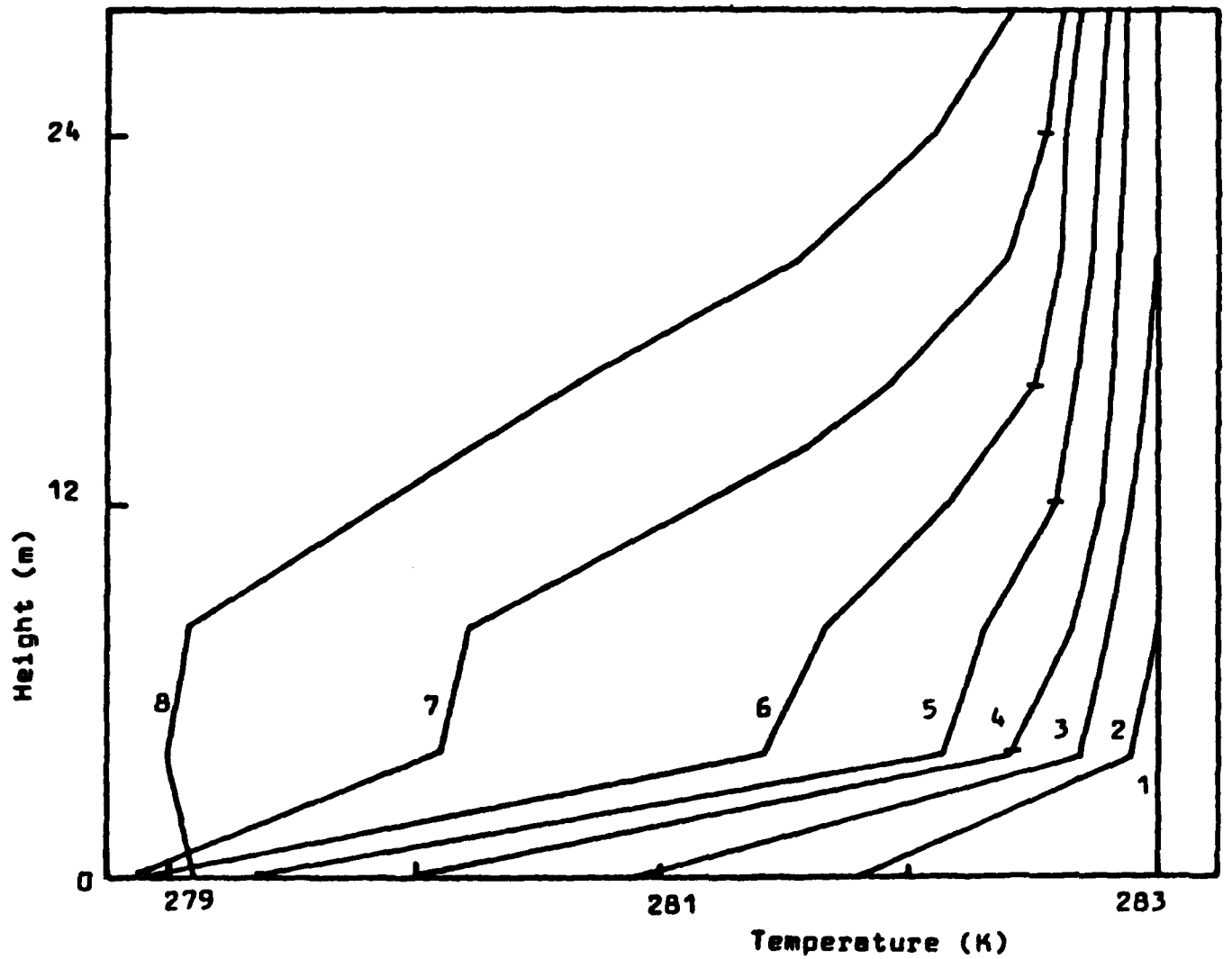

Figure 2: Temperature evolution in the boundary layer over a dry clay soil with an initial isothermal atmosphere of 283K

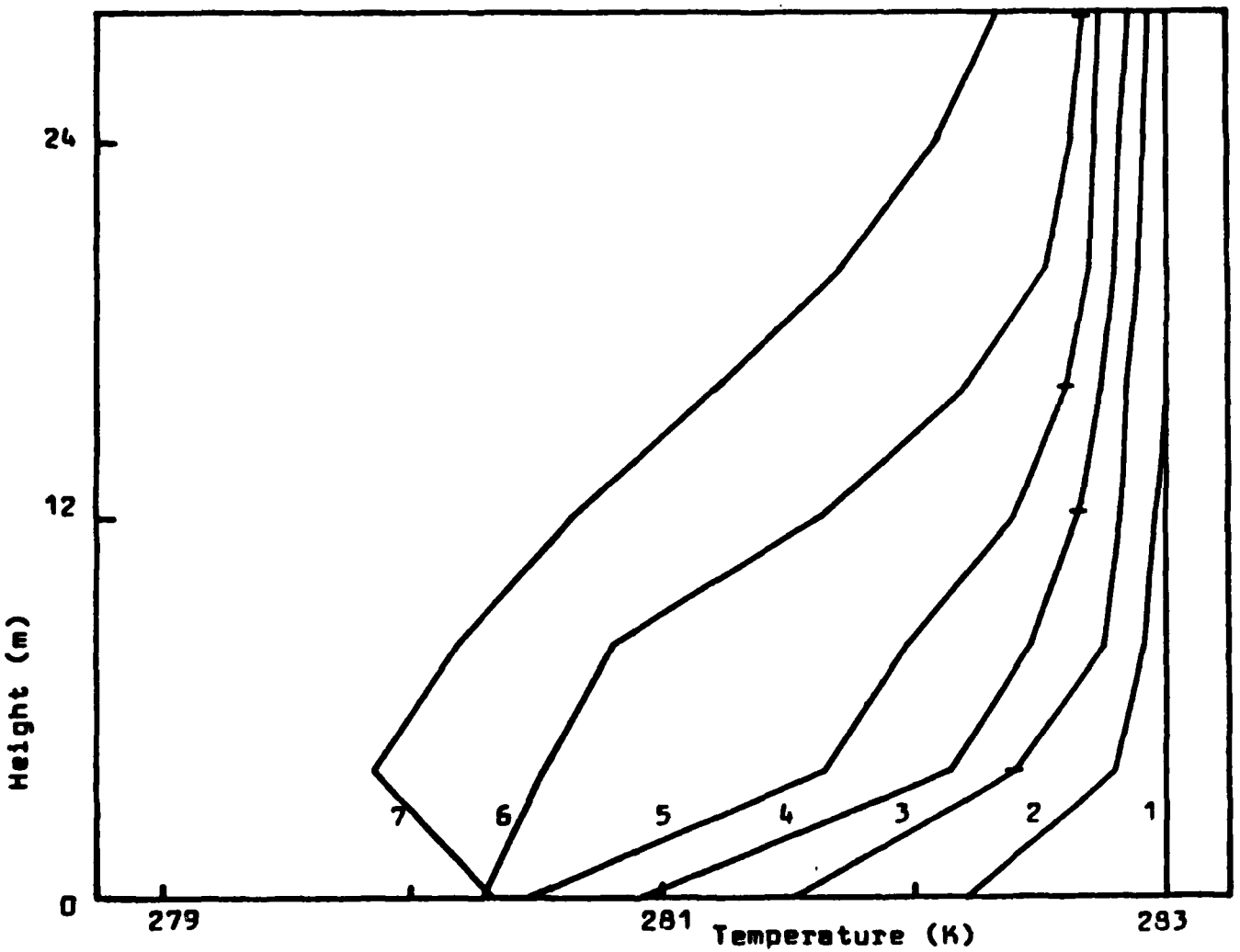

Figure 3: Temperature evolution in the boundary layer over a dry clay soil, including the effect of a vegetation minimum in temperature, with an initial isothermal atmosphere of 283K

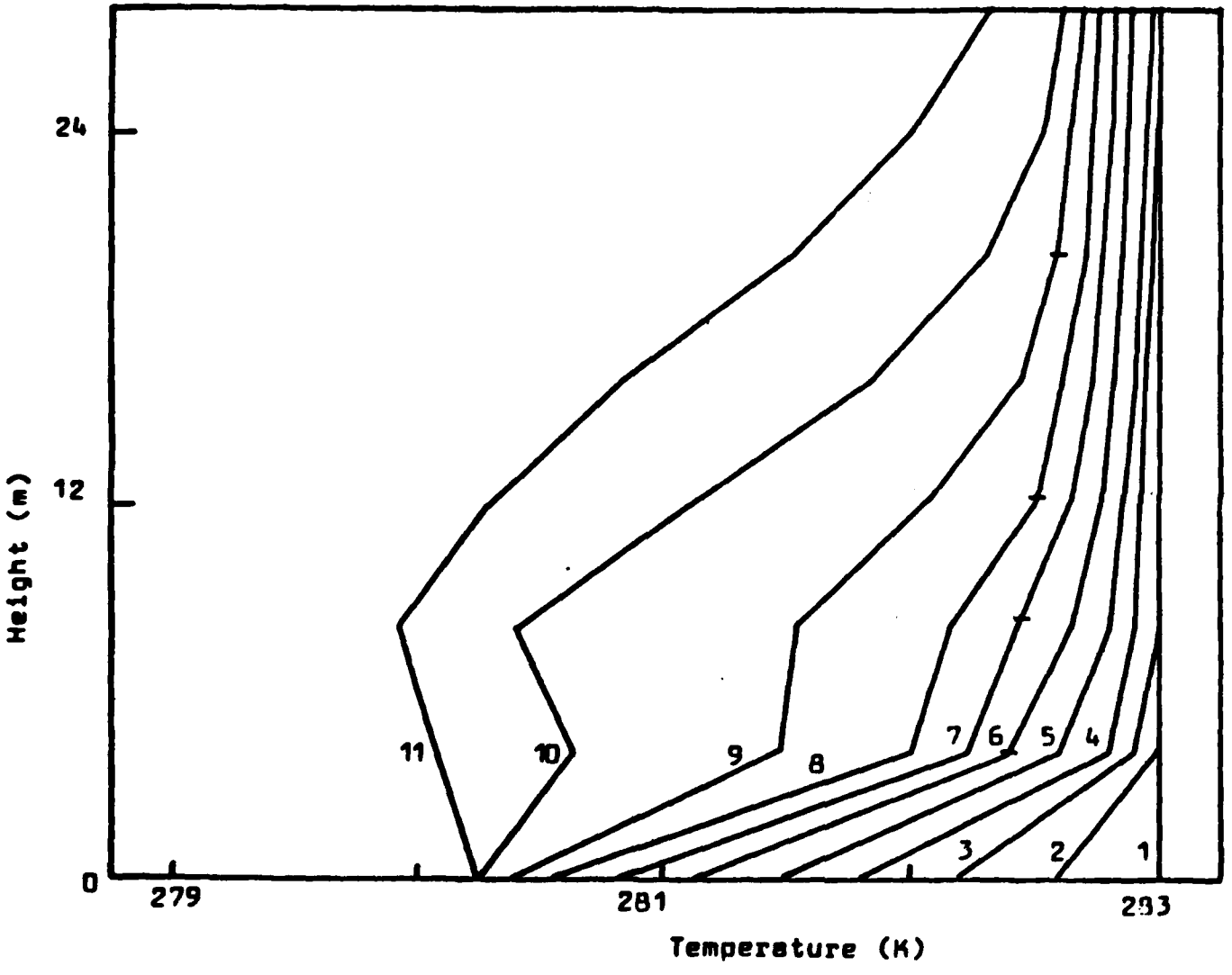

Figure 4: Temperature evolution in the boundary layer over a wet clay soil with an initial isothermal atmosphere of 283K

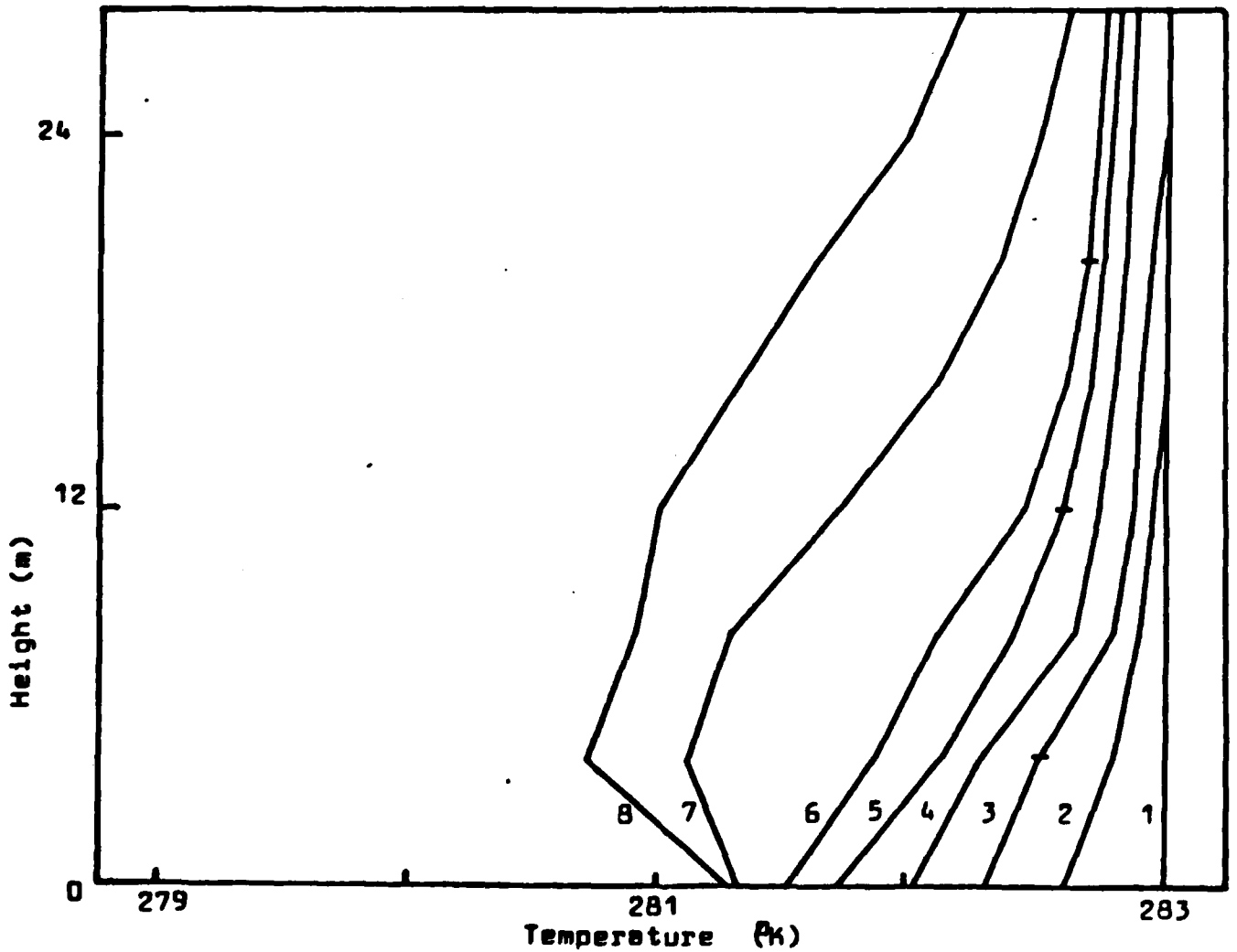

Figure 5: Temperature evolution in the boundary layer over a wet clay soil, including the effect of a vegetation minimum in temperature, with an initial isothermal atmosphere of 283K

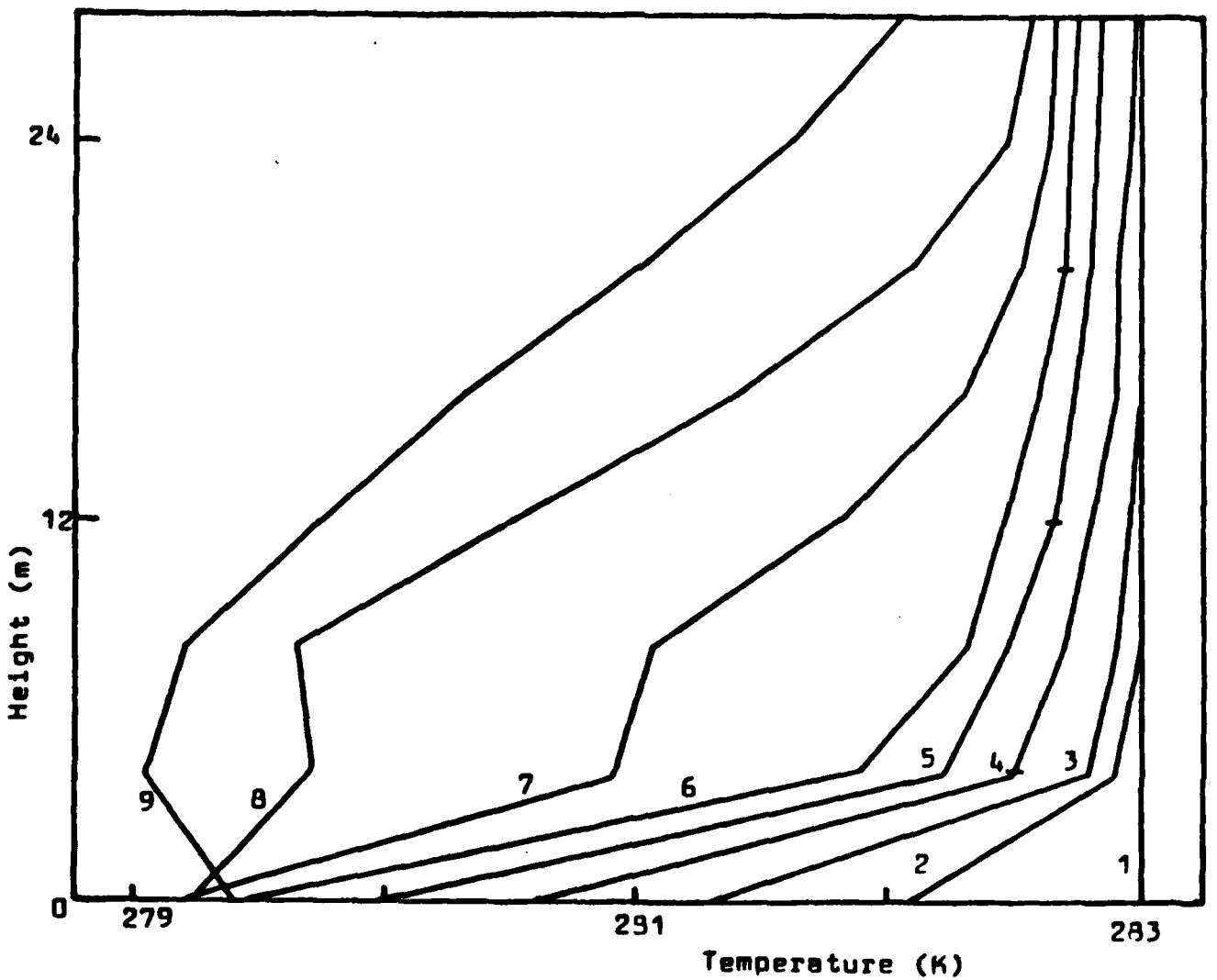

Figure 6: Temperature evolution in the boundary layer over a dry sand soil with an initial isothermal atmosphere of 283K

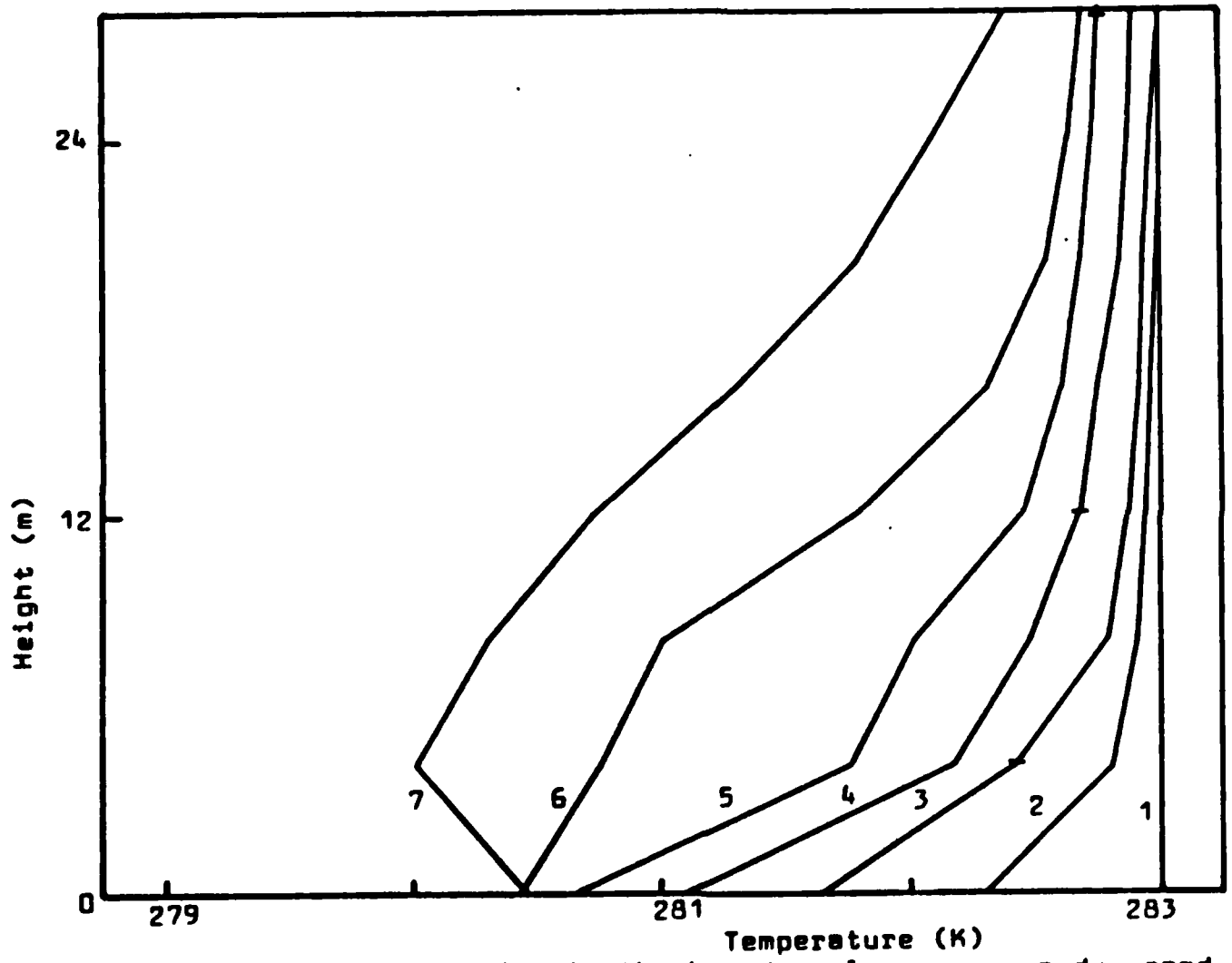

Figure 7: Temperature evolution in the boundary layer over a dry sand soil, including the effect of a vegetation minimum in temperature, with an initial isothermal atmosphere of 283K.

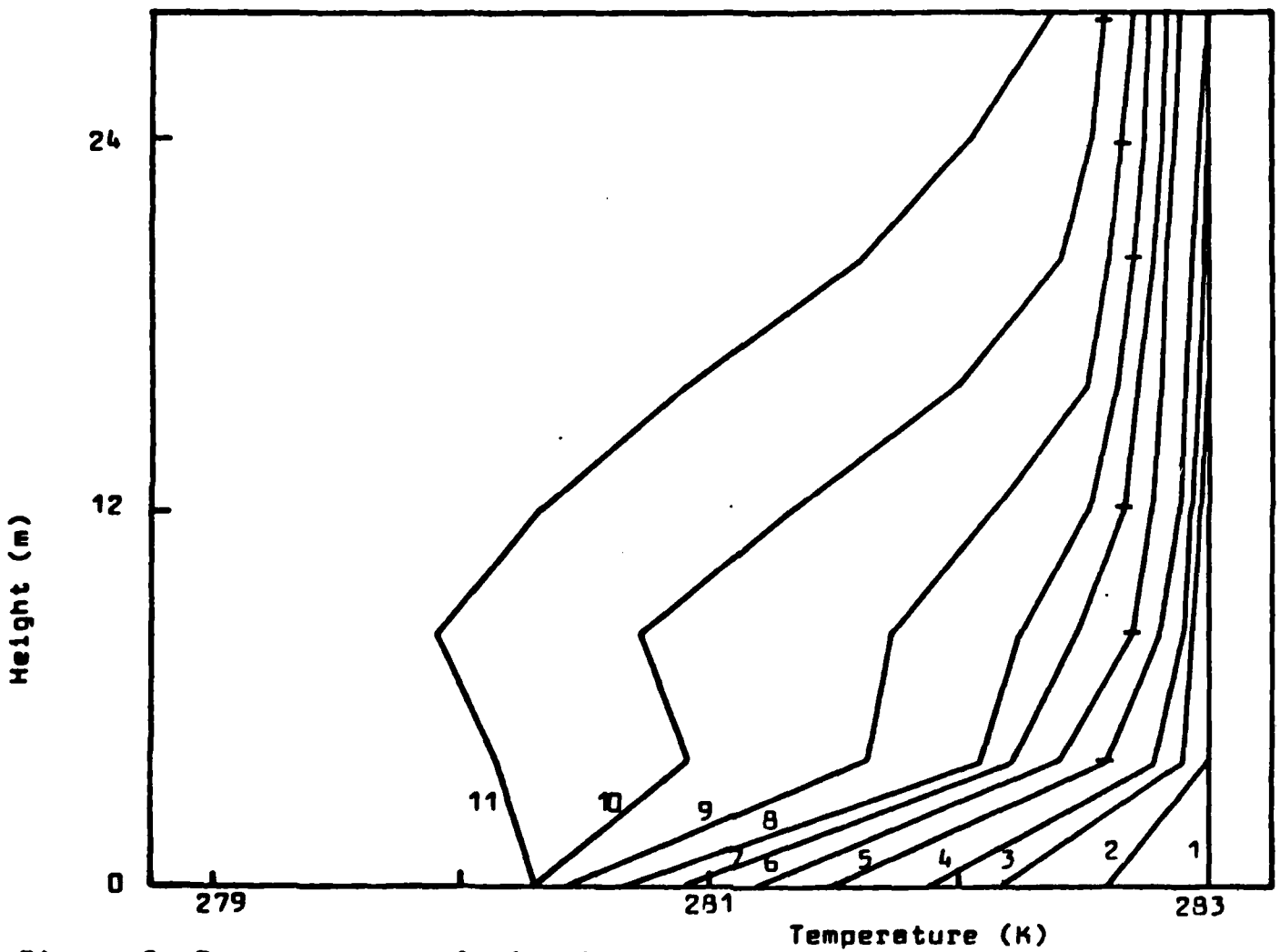

Figure 8: Temperature evolution in the boundary layer over a wet sand soil with an initial isothermal atmosphere of 283K.

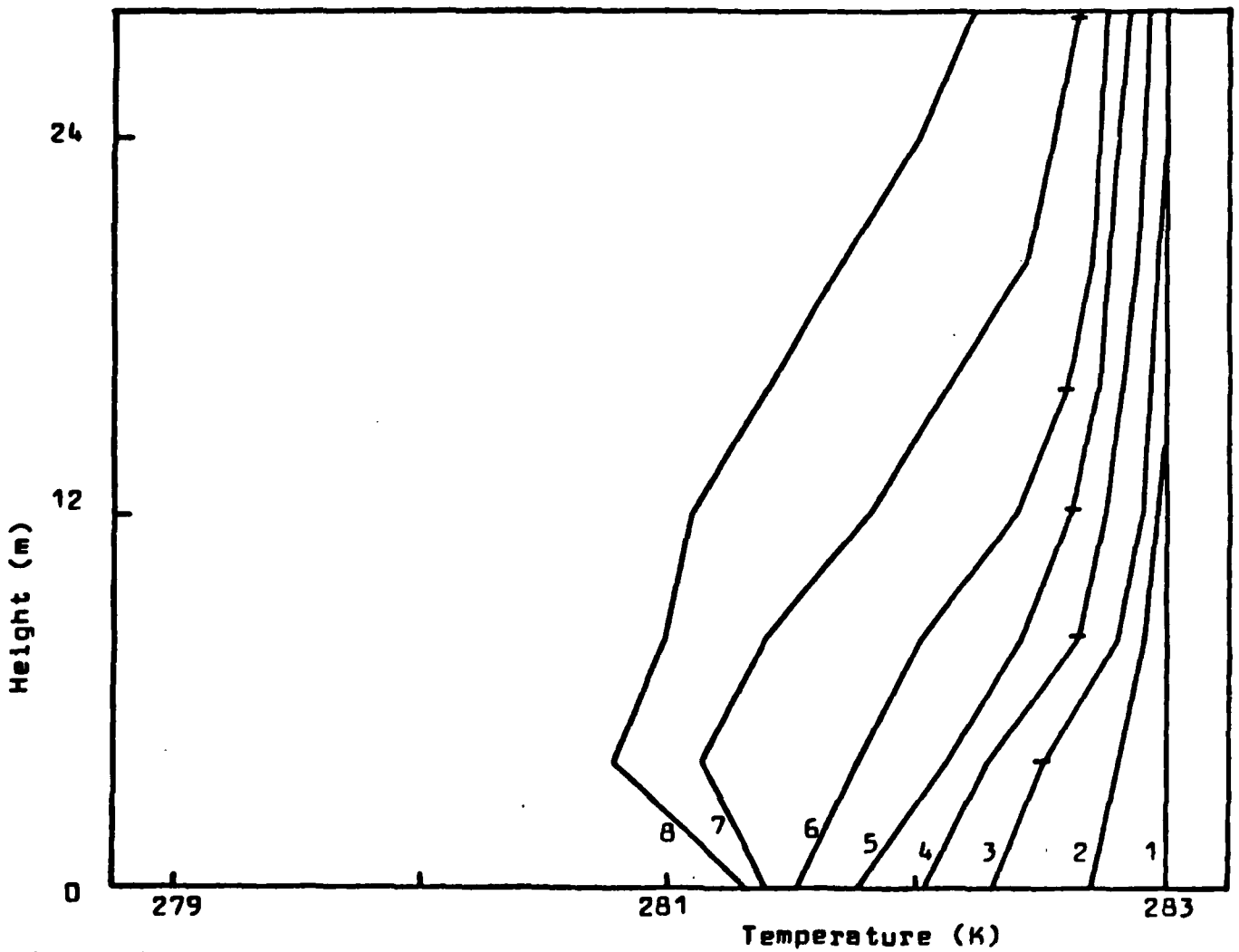

Figure 9: Temperature evolution in the boundary layer over a wet sand soil, including the effect of a vegetation minimum in temperature, with an initial isothermal atmosphere of 283K.

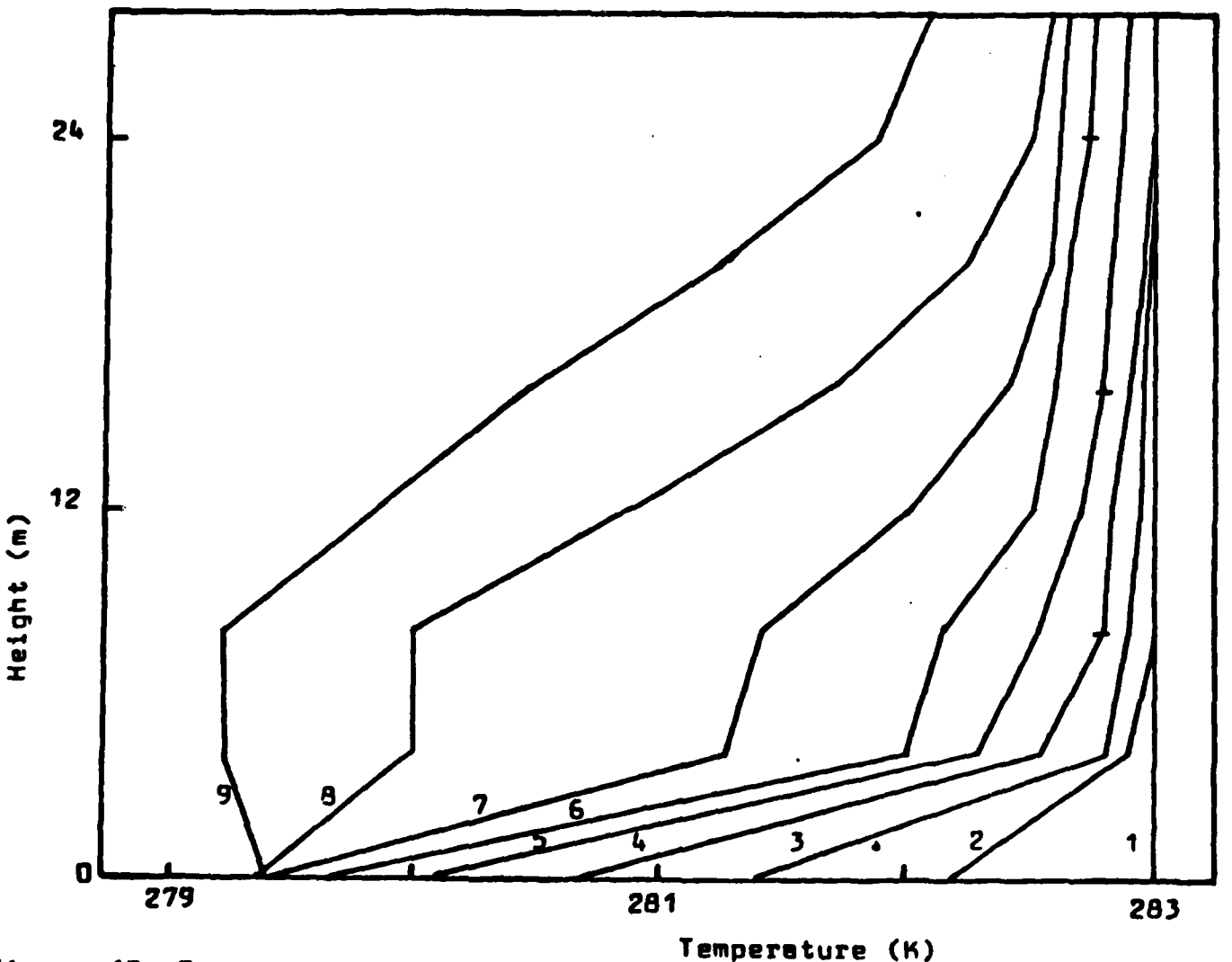

Figure 10: Temperature evolution in the boundary layer over an old snow cover with an initial isothermal atmosphere of 283K

END

FILMED

9-85

DTIC